The promiscuity of alkaline phosphatase against nucleotides and sugar phosphates. Computational analysis and kinetics.

Borgþór Pétursson

Raunvísindadeild
Háskóli Íslands
2014

The promiscuity of alkaline phosphatase against nucleotides and sugar phosphates. Computational analysis and kinetics.

Borgþór Pétursson

15 eininga ritgerð sem er hluti af
Baccalaureus Scientiarum gráðu í lífefnafræði

Leiðbeinandi
Bjarni Ásgeirsson

Aðstoðarleiðbeinandi
Hörður Filippusson

Raunvísindadeild
Verkfræði- og náttúruvísindasvið
Háskóli Íslands
Reykjavík, september 2014

The promiscuity of alkaline phosphatase against nucleotides and sugar phosphates. computational analysis and kinetics.

15 eininga ritgerð sem er hluti af *Baccalaureus Scientiarum* gráðu í lífefnafræði

Raunvísindadeild
Verkfræði- og náttúruvísindasvið
Háskóli Íslands
Dunhagi 3
107 Reykjavík

Sími: 525 4000

Skráningarupplýsingar:
Borgþór Pétursson, 2014, The promiscuity of alkaline phosphatase against nucleotides and sugar phosphates. Computational analysis and kinetics, BS ritgerð, Raunvísindadeild, Háskóli Íslands, 57 bls.

Prentun: Háskólaprent
Reykjavík, september, 2014

Útdráttur

Alkalískir fosfatasar eru algeng prótín í náttúrunni sem hvata vatnsrof fosfathópa. Þeir sýna því umtalsverða fjölvirkni gagnvart hinum ýmsu efnum t.d. núkleótíðum og fosfatsykrum og hafa alkalískir fosfatasar verið notaðir til þess að affosfórýlera núkleótíð svo sem ATP. Árið 2008 höfðu þau Bjarni Ásgeirsson og Guðrún Jónsdóttir rannsakað fjölvirkni alkalískra fosfatasa úr *Vibrio* sjávarörveru, *E.coli*, kálfi og þorski. Niðurstaða þeirrar rannsóknar var sú að alkalískur fosfatasi úr *Vibrio* gat ekki affosforýlerað ADP og ATP en affosforýleraði hinsvegar AMP. Aftur á móti gat alkalískur fosfatasi úr *E. coli* affosforýlerað AMP, ADP og ATP.

Markmið þessa BS verkefnis var að kanna aftur fjölvirkni alkalísks fosfatasa úr *Vibrio* og *E. coli* til staðfestingar með því að mæla styrk ólífræns fosfats sem myndaðist eftir hvarf fosfatasanna við núkleótíðin með annarri aðferð en Guðrún Jónsdóttir hafði notað. Einnig voru gildin K_m og k_{cat} ákvörðuð með Michaelis-Menten hraðafræði. Stuðst var við tölvulíkönin AutoDock Vina og PyMol til þess að skýra mismunandi sértækni ensímana.

Niðurstaðan var sú að enginn munur var á sértækni ensímanna með tilliti til núkleótíðanna. Aftur á móti var munur á hraðaföstunum enda munur á stellingum hvarfefna í hvarfstöðvum ensímana samkvæmt tölvulíkaninu.

Abstract

Alkaline phosphatases are widely found in nature and their primary function is to catalyze the hydrolysis of phosphate-groups. They are promiscuous towards various substrates such as nucleotides and phosphate-sugars and are used for dephosphorylation of nucleotides like ATP. In 2008, Bjarni Ásgeirsson and Guðrún Jónsdóttir conducted an experiment on the promiscuity of alkaline phosphatases found in a *Vibrio* deep-sea microbe, *E. coli*, calf and cod. They found that alkaline phosphatase from *Vibrio* was unable to cut ADP and ATP while being able to dephosphorylate AMP. However, according to their result alkaline phosphatase from *E. coli* was able to dephosphorylate AMP, ADP and ATP.

The aim of this B.Sc. project was to repeat the experiment for confirmation by using another method to determine the concentration of inorganic phosphate released by the reaction catalyzed by the alkaline phosphatase and determine the K_m and k_{cat} with Michaelis-Menten kinetics. The docking program AutoDock Vina was used to help explaining the difference in the enzymes specificity while the results were viewed in PyMol.

The results showed that there was no difference in specificity between the two enzymes when it came to dephosphorylation of the three nucleotides. However, there was a difference between the rate constants of the enzymes as there was a difference between the conformations of substrates inside the enzymes' active sites according to the computer model

Table of Contents

Figures

Tables

Abbreviations

VAP- *Vibrio* alkaline phosphatase

ECAP – *E. coli* alkaline phosphatase

PLAP - Placental alkaline phosphatase

IAP – Intestinal alkaline phosphatase

SAP- Shrimp alkaline phosphatase

AMP- Adenosine monophosphate

ADP- Adenosine diphosphate

ATP- Adenosine triphosphate

PCR- Polymerase chain reaction

CAPS- N-cyclohexyl-3-aminopropanesulfonic acid

Thanks

I would like to thank Bjarni Ásgeirsson for his help and guidance in this project. I would also like to thank Hörður Filippusson for his help.

I also would like to thank friends and family for their support.

Introduction.

1.1 Protein promiscuity.

Many enzymes have the ability to promiscuously catalyze reactions involving substrates other than those for which they evolved. This ability has been traced to the evolvability of proteins, as promiscuous activities can be seen as a starting point for new functions[1].

The degree of promiscuity is determined by the diversity of promiscuous activities, for example how many types of bonds are being broken or formed and if there is any difference in reaction mechanism between the native and promiscuous reaction. The magnitude of promiscuity is often described in terms of the relative kinetics of the promiscuous activity (in k_{cat} and K_m) to the native substrates. The order of the magnitude of promiscuous activity is usually more varied compared to that of the native substrates[2].

1.2 Adaptation of enzymes to temperature.

Temperature is an important environmental factor that affects living organisms as it affects the kinetic energy of molecules including bioorganic ones such as proteins. It affects the strength of interactions between molecules and thus the rate of collisions and reactions. The most dominant effect is the effect on protein stability. Proteins unfold when the temperature exceeds the T_m (melting temperature) of the protein. Adaptation to extreme temperatures, therefore, results in enzymes with suitable T_m values. Such enzymes also exhibit rate-temperature profiles such that the maximum rate for said enzyme occurs close the growth temperature of the living organism. Thermophilic (adapted to $\geq$ 60°C)[3], mesophilic (25-50°C)[4] and psychrophilic (around 5-25°C)[4] organisms seem to have similar catalytic efficiencies (k_{cat}/K_M) at their respective operating temperatures. However, thermophilic enzymes have lower catalytic rates than mesophilic enzymes at moderate temperatures due to their rigidity and compactness. Psychrophilic enzymes on the other hand exhibit high flexibility to adjust to low temperatures[5].

The empirical measure used to compare the rate-temperature between the three environmental classes is Q_{10} (fold increase in rate-temperature per 10°C). The Q_{10} does not seem to differ greatly between the three environmental groups and it seems to be around 1.8 in all cases. So the three groups do not have unique rate-temperature dependencies or active site dynamics[6].

Figure 1 below compares the temperature dependencies of activity, efficiency and specific activity between the three environmental classes and non-enzymatic reactions (k_{non}).

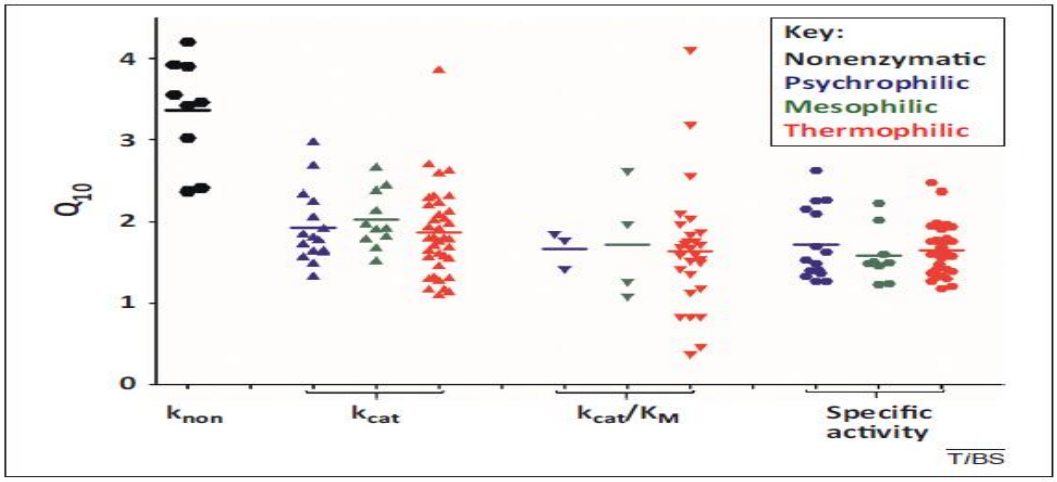

Figure 1: Temperature dependencies of enzyme catalyzed reactions. Q_{10} for the reaction rates k_{cat}, catalytic efficiencies and specific activities of the three environmental groups means and standard deviation for each group are respectively: psychrophilic (n= 34, mean = 1.81, SD = 0.43), mesophilic (n = 24, mean = 1.81 SD= 0.44), thermophilic (n= 100, mean = 1.73 and SD = 0.65)[6].

1.3 Phosphoryl group transfers and ATP

ATP can be seen as the energy currency of cells. The free energy surplus from the metabolism of nutrients in heterotrophic cells is used to form ATP from ADP and P_i. ATP then donates some of its energy to endergonic processes for example synthesis of metabolic intermediates and macromolecules as well as transport of

substances across membranes against concentration gradient. Usually, the final result is the conversion of ATP to ADP, or even AMP. The hydrolysis of ATP has a large negative free energy change (-30.5 kJ/mol under standard conditions) even though the breaking of the bonds requires energy input as it separates one of the phosphates from the other two negatively charged phosphates, it enables the P_i to form several resonance forms. This means ATP is a high energy phosphate compound. Under intracellular conditions the phosphorylation potential

$$\Delta G_p = G'^{\circ} + RTln\frac{[ADP][P]}{[ATP]} \qquad \textbf{(1)}$$

is different due to difference in ATP concentration between cell types, difference in metabolic condition, pH etc. From equation (1) one can deduce that the higher ATP concentration the more negative the phosphorylation potential. Therefore, living cells have developed metabolic pathways which maintain a high ATP concentration. Examples of reactions in which hydrolysis of ATP fuels the process are muscle contraction and movement of enzymes along DNA.

Usually simple hydrolysis of ATP only releases heat which cannot be harvested to drive chemical reaction in an isothermal system. Usually, the ATP molecule is transferred to other molecules such as an amino acid residue in an enzyme where this part of the ATP is covalently attached to the residue. ATP phosphoryl transportation is widely used within in the cell. One important example is when ATP carries energy from high-energy phosphate compound to compound such as glucose rendering them more reactive.

An important feature of the ATP molecule is that it is kinetically stable even though thermodynamically it is not. Because of it high activation energy (200-400 kJ/mol) necessary for uncatalized cleavage of the phosphoanhydride bonds[7].
In this project, we compared the rate of dephosphorylation between the cold-adapted *Vibrio* alkaline phosphatase and alkaline phosphatase from *E. coli* bacteria.

1.4 Alkaline phosphatase

Alkaline phosphatase (will also be referred to as AP) is widely found in nature and generally has a dimeric structure although there are indications that multimeric or monomeric forms exist in bacteria[8]. AP shows broad substrate specificity and catalyzes the hydrolysis or transesterification of phosphoryl esters. APs are extracellular and contain magnesium and zinc ions for stability and activity. Their main function in bacteria is to provide inorganic phosphate as they catalyze the hydrolysis of phosphoryl esters[9].

The enzymes have a highly conserved sequence so it can be assumed that AP found in other organisms have a similar overall structure and reaction mechanism even though vertebrate APs tend to have much higher catalytic activity. The most prominent difference between the primary structures of vertebrate APs and *E. coli* AP is that of the loop regions which have grown either smaller or larger and the metal ion binding residues do also vary slightly being for the most part identical[10]. The comparison between alkaline phosphatase from human placenta, yeast and *E. coli* have shown that in these three APs, the most significant differences are the positioning of the bound phosphate and the metal in the third binding site (normally Mg)[11] . However, mammalian APs have also higher K_m and have higher optimum pH and display lower heat stability[12]. Mammalian APs have broad substrate specificity but to-date only few of the compounds hydrolyzed or transphosphorylated *in vitro* have been confirmed to serve as natural substrates. The active site is shallow and only the phosphoryl group enters amongst the catalytic residues. It is more the steric access that determines the specificity [12].

1.5 *Vibrio* alkaline phosphatase.

Vibrio alkaline phosphatase is a cold-adapted alkaline phosphatase found in the North-Atlantic bacterium. Its polypeptide chain is the longest of all alkaline phosphatases and its activity (k_{cat}) is among the highest[13].

VAP (*Vibrio* alkaline phosphatase) is a dimer. Each monomer contains two zinc atoms and one magnesium ion. The three metal ions play an important role in the catalysis and the magnesium is stabilizing for the structure as well as it abstracts the proton from the nucleophilic serine as it forms a metal-bound hydroxyl ion. All-zinc containing enzymes have lower activity but they can be reactivated when magnesium is added at alkaline pH. There are three water molecules in the active site and they are believed to take part in the catalytic function and their location might influence the proficiency of the catalysis. VAP has a slightly more positive potential area surrounding the active site compared to ECAP (*E. coli* alkaline phosphatase) and PLAP (Placental alkaline phosphatase). Possibly this serves to attract negatively charged substrates into the active site. This is an interesting feature since a very negatively charged surface has been observed in some cold–adapted enzymes. The active site is shielded by two of the four inserts found in the structure. These inserts might regulate the interactions of VAP with various substrates.

The mobility of the key residues (the ones involved in the reaction) is an important factor when it comes to understanding the subtle differences between alkaline phosphatase variants which renders them (in this case) specifically cold-active. The nucleophilic serine 65 is on a helix which superimposes neatly onto a corresponding ECAP helix. The serine 65 residue has a flexible nature as it is refined in two separate conformations in the VAP crystal. Another key active-site residue is arginine 129 that superimposes well onto the corresponding residue in ECAP and PLAP and the docked conformation in SAP (shrimp alkaline phosphatase)[13].

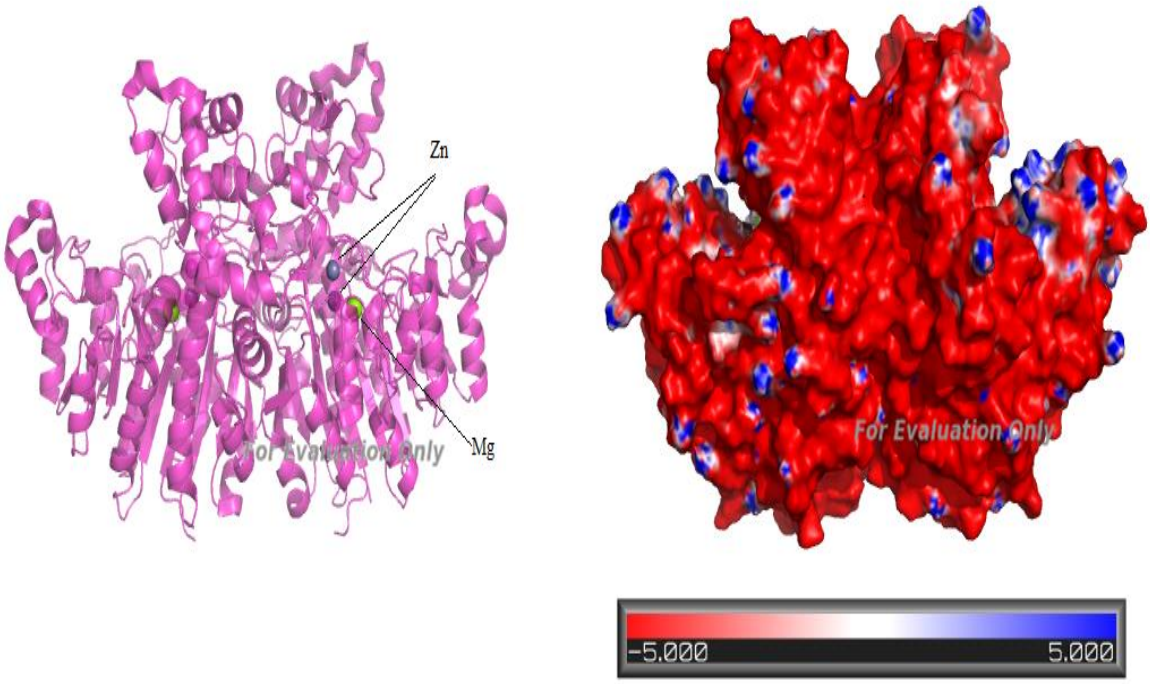

Figure 2: Vibrio alkaline phosphatase shown as cartoon with visible metal ions on the left and Vibrio alkaline phosphatase shown with electro static surface on the right. The bar below shows the electrostatic potential. Each color represents (k_b T e^{-1}) where k is the Boltzman constant, T is 300 Kelvin and e is the charge of an electron. The resolution of the structure is 1.4 Å [13].

1.6 *E. coli* alkaline phosphatase

Unlike the *Vibrio* alkaline phosphatase, the *E .coli* alkaline phosphatase (ECAP) is not cold-adapted and is, therefore, expected to have a more rigid active site and is not as active as VAP. It contains 450 amino acids and its molecular weight is 47,230 (Da). Like VAP, ECAP has two active sites though only one is active at a time[14,15]. ECAP's active site contains three metal ions, two Zn^{2+} and one Mg^{2+} , which are crucial for its activity and a stable apoenzyme can be reactivated with Zn, even Co restores significant activity [16]. ECAP has an optimum pH at 8.0 and an isoelectric point at pH 4.5[17]. Studies on activity show that ECAP binds

phosphate tightly over a wide range of pH and forms complexes that perhaps are intermediates in the hydrolysis [18].

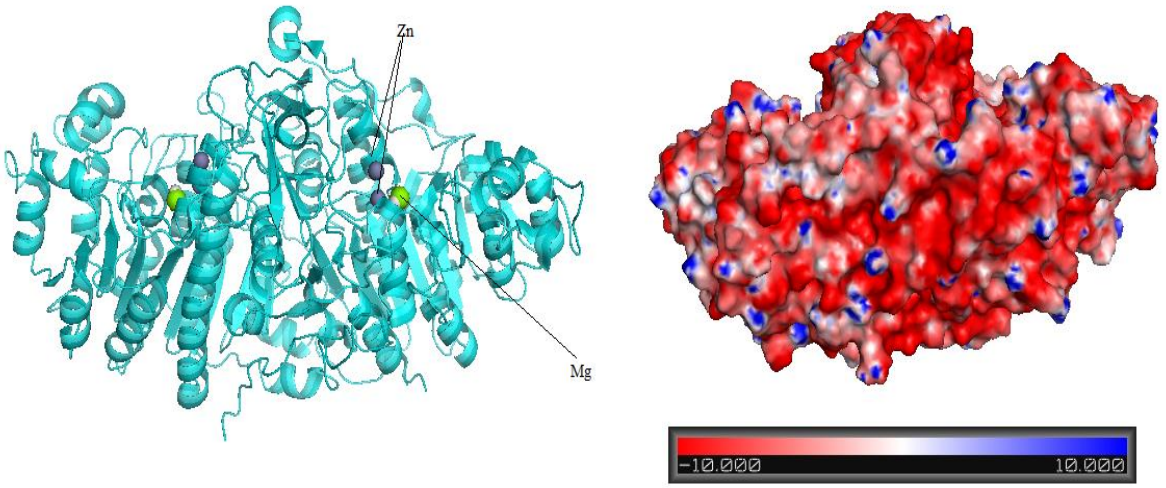

Figure 3: E. coli alkaline phosphatase shown as cartoon with visible metal ions on the left and E. coli alkaline phosphatase shown on the right with electrostatic surface. The bar below shows the electrostatic potential each color represents (k_b T e^{-1}) where k is the Boltzman constant, T is 300 Kelvin and e is the charge of an electron. The resolution of the structure is 1.75 Å[19].

1.7 Nucleotide degradation by the alkaline phosphatase.

Intestinal alkaline phosphatase (iAP) seems to have considerably higher activity towards ATP compared to ADP and AMP[20]. Furthermore, the activity and dissociation constant increase at a more alkaline pH around 9 (compared to pH 6 and 7.4). The figure below shows the results from a study conducted by Christine M. Kaufman et al. in 2014 where the activity of intestinal alkaline phosphatase was tested against AMP, ADP and ATP at pH 6, 7.4 and 9. According to their results iAP had higher activity towards ATP and ADP than AMP and the difference between the nucleotides got greater at a more alkaline pH (9 versus 6 and 7.4)[20].

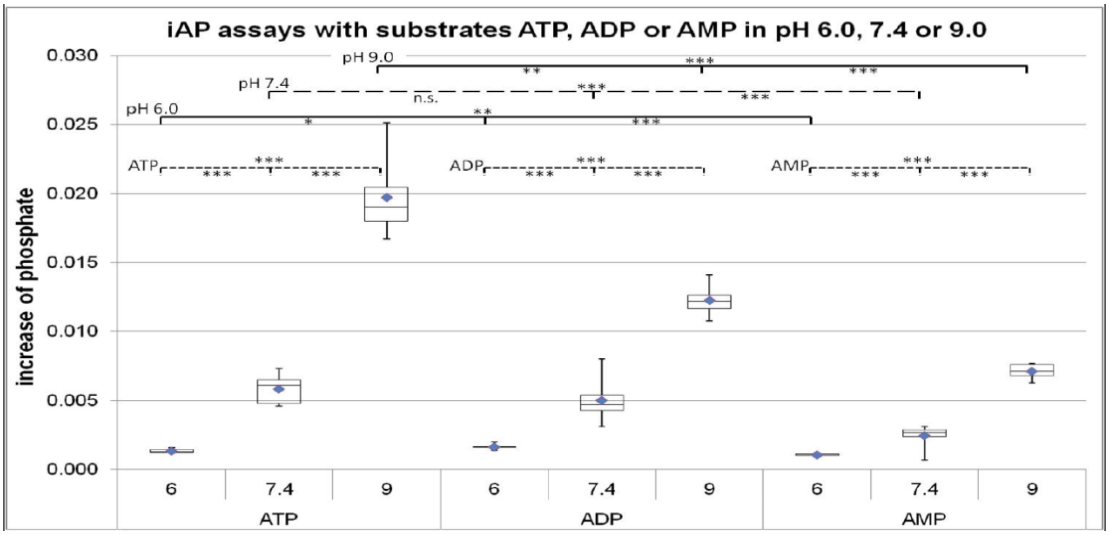

Figure 4: Box-whisker plot of the values of the slopes of linear trend lines of initial phosphate increase. The change was measured to determine the activity of intestinal alkaline phosphatase towards the nucleotide-phosphates. The enzyme turned out to be more active towards ADP and ATP as there was higher increase in release of phosphate. The increase of phosphate was photometrically detected[20].

However, according to another study, Chappelet Tordo observed a higher activity toward AMP compared to ATP at pH 10 and comparable activity at pH 8[15]. This indicates a preferred degradation of AMP at pH 10. It has been demonstrated, however, that many factors like the type of buffer and ionic strength influence the activity and specificity of intestinal alkaline phosphatase. Ions like Mg^{2+} or Zn^{2+}reverse the order of activity. Additionally, application of buffers containing Tris at pH 8 and ethanolamine at pH 10 results in lower levels of detectable phosphate with ATP since these additives are good phosphate acceptors[20].

1.8 Alkaline phosphatase phosphoryl transfer of ATP and health.

Alkaline phosphatase plays an important role in maintaining human health. For instance, iAP (intestinal alkaline phosphatase) promotes the growth of the various bacteria which inhabit the intestines. Normally, around 10^{14} bacteria of 300-1000 species inhabit the human gut[21]. They contribute to human health by playing their part in, among other things, vitamin synthesis, food digestion and the immune system[22-25]. Dysregulation of the normal homeostasis of the intestinal microbiota results in great many diseases such as metabolic syndrome, cancer and obesity. Alkaline phosphatase maintains the bacterial flora since ATP inhibits bacterial growth, especially of gram positive bacteria, in the intestines even at low concentration while ADP, AMP and phosphate cause little to no inhibition of the growth of bacteria. Figure 5 shows how ATP might affect the growth of bacteria in the intestines.

Other nucleotide-triphosphates decrease bacterial growth as well. IAP does not affect bacterial growth directly but rather it dephosphorylates nucleotide triphosphates which indicate that these molecules are intestinal alkaline phosphatase targets. This raises the question if nucleotide triphosphates prevent bacterial growth elsewhere and that other APs play similar role in bacterial homeostasis. Furthermore, iAP plays an important role in fat absorption and recent studies show that IAP prevented high fat diet metabolic syndrome in mice[26].

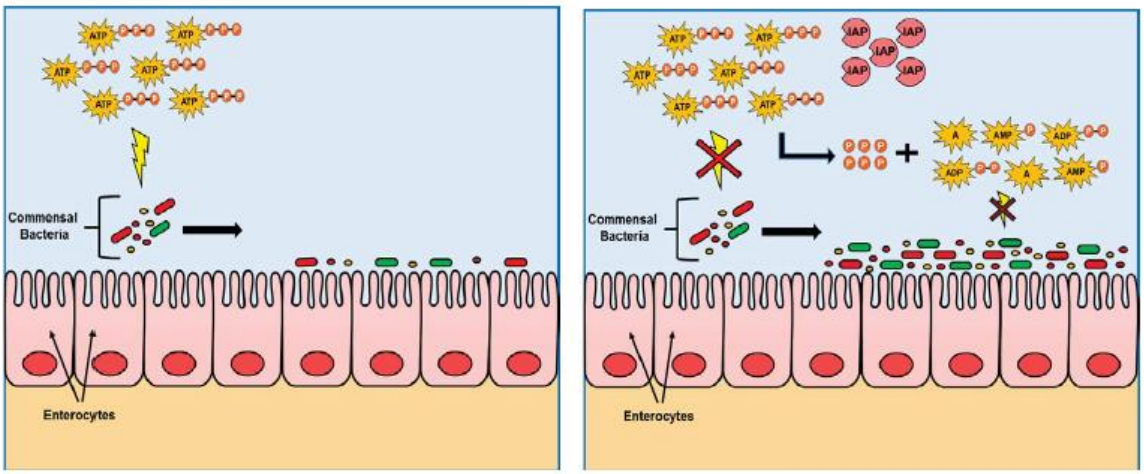

Figure 5: This figure shows the effect iAP has on bacterial growth. IAP hydrolyses ATP molecules and thus protects the intestinal bacterial growth since ATP is known to inhibit the bacterial growth in the intestines while AMP and ADP cause little or no inhibition[26].

1.9 Docking

Since the amount of molecular biological data available has been expanding, the use of computer based analysis of molecular interaction such as protein-ligand binding becomes more necessary. For this purpose, docking algorithms have to include a reasonably accurate model of energy and the flexibility of molecules[27].

Docking is a computational method used for predicting the non-covalent bindings between macromolecules or macromolecule (such as proteins) and a much smaller ligand. Starting with the unbound structures which are acquired from homology modeling or other structure determination[28].

Protein- ligand docking models optimize the binding of a ligand into an active site of a protein. The contact surfaces between the ligand and the protein are relatively small, much smaller than in protein-protein docking. In this case, the main challenge is the ligand‘s flexibility as it can conform to the protein‘s surface in many ways. Computational methods are then used to predict the binding affinity

and the conformation of the ligand[27]. This technique is used to obtain leads for medical development as drug-like molecules are screened with this method.

Docking programs usually use a scoring function in order to recreate the chemical potentials which predict the conformation of binding. Superficial physics- based (Coulombs energy and van der Waals forces) need to be empirically weighted to account for the difference in energy and free energy. Receptor usually have to be prepared by adding hydrogens and charges select site and remove/include water and cofactors [28].

1.10 AutoDockVina

For this project I decided to use AutoDockVina since it is accessible, free and yet precise. Designed and implemented by Dr. Oleg Trott in the Molecular Graphics Lab at The Scripps Research Institute. Other software such as Autodock, and Molegro are also available.

The scoring function of Vina is more of the machine learning type rather than direct use of physics based scoring.

The function used for the conformationally-dependent part of the scoring is:

$$\sum_{i<j} f_{t_i t_j} r_{ij} \qquad (2)$$

This is a summation over all the pairs of atoms which can move relative to one another. Each atom i is here assigned a type t_i and a symmetric set of the interaction function f over distance r (r_{ij}) being the distance between atoms i and j.

f is defined relative to the surface distance:

$$f_{t_i t_j}(r_{ij}) \equiv h_{t_l t_j}(d_{ij}) \qquad (3)$$

Where h is weighted sum of steric interactions.

$$\boldsymbol{d_{ij} = r_{ij} - R_{ij} - R_{ij},} \qquad \textbf{(4)}$$

where R_t is the van der Waals radius of atom type t.

The hydrophobic value is extrapolated on the scale where hydrophobicity equals 1 when d is less than 0.5 Å but 0 at more than 1.5 Å.

This value can be seen as the sum of inter-molecular and intra-molecular inter action

$C = c_{intra} + c_{inter}$ (5)

The algorithm of AutoDockVina then tries to find the global minimum of C. Additionally it finds and ranks other suitable conformations.

The free energy of binding is calculated from the lowest inter-molecular score of conformation here referred to as l.

$s_1 = g(c_1 - c_{intra1} = g(c_{inter1})$ (6)

Where g is an arbitrary strictly increasing smooth function (possibly non-linear).

The output also shows other low –scoring conformation.

$s_i = g(c_i - c_{intra1})$ (7)

The conformationally independent function g is defined as:

$g(c_{inter}) = \frac{c_{inter}}{1+wN_{rot}}$ (8)

Where N_{rot} is the number of active rotatable bonds between heavy atoms in the ligand while w is the associated weight[28].

2. Materials and Methods.

2.1 Materials.

Ammonium molybdate and $CuCl_2$were bought from Acros Organic (New Jersey, United States). IgG:HAS, 2-mercatoethanol, Coomassie-Brilliant-Blue, isopropanol, perchloric acid, sulphuric acid, *E. coli* alkaline phosphatase, adenosine diphosphate, adenosine monophosphate, CAPS, adenosine triphosphate and pNPP were obtained from Sigma Aldrich (St. Louis, USA). Ethylene acetate was obtained from Pierce Chemical Company (Rockford, USA). NaCl was obtained from Fisher Scientific. $MgCl_2$ was obtained from Merck (Darmstadt, Germany). VAP alkaline phosphatase was prepared as described previously[29].

2.2 Determination of phosphate concentration

0.1 M CAPS buffer with 1 mM $MgCl_2$ and 0.5 M NaCl at pH 9.8 was used as a solvent for both protein and nucleotide phosphates.

Ammonium molybdate was used to measure the free inorganic phosphate concentration. Molybdate is acidic and that causes ATP to be unstable in its presence. Therefore, it is vital to separate the molybdate from the ATP molecules by extracting the molybdate-phosphate complex into ethyl acetate[30].

The determination of phosphate concentration was done in the following way:

1. A 60 mM molybdate solution was prepared (with 0.27 M NaCl). The solution was shaken (manually) at around 45 °C. The solution needed to be fresh in order for the molybdate to stay dissolved.

2. 750 µl of the molybdate solution was added to the test tube (containing 750 µl sample and 250 µl and perchloric acid). The test tube was shaken with a vortex stirrer.

3. 2 ml of ethyl acetate was added to the test tube. The solution was stirred with a vortex stirrer for at least 40 seconds and the solutions allowed to separate.

4. One ml of the organic layer was added to another test tube with 2 ml of an isopropanol solution (with 0.06 mM $CuCl_2$ and 0.27 M H_2SO_4).

5. 2.5 µl of 2-mercaptoethanol were added to the test tube.

6. The solution was stirred with a vortex stirrer and the absorption was measured at 625 nm after waiting for 5 minutes for the absorption to peak.

2.3 Preparation of the phosphate standard curve.

A 2 mM phosphate solution was prepared and then serially diluted (1, 1/2 to 1/256). After that, the absorbance at each concentration was determined with the procedure described above and the absorption of de-ionized water was used as a blank.

2.4 Determination of protein concentration.

The Zaman and Verwilghen (1979) method used here is a variant of the Bradford method (1976) IgG:HSA was used as a standard . The protein standard was diluted to 400 µg/ml and then serially diluted to 40 µg/ml with six points in between. Two hundred and fifty µl of these samples were then added to 2.75 ml of Coomassie blue solution. A blank was prepared by adding 250 µl of distilled water to 2.75 ml of Coomassie blue solution. After 5-10 minutes the absorption was measured at 620 nm. When determining the protein concentration of samples used in the project 250 µl of the protein solution (VAP or ECAP in 0.1 M CAPS buffer with 1 mM $MgCl_2$, and 0.5 M NaCl at pH 9.8) were added to 2.75 ml of Coomassie blue solution and measured the absorption at 620 nm against a blank with 250 µl in 2.75 ml of Coomassie blue solution. The equation of the standard curve was used to determine the concentration of individual samples.

2.5 Measurements of enzyme activity.

Beforehand, the activity of ECAP and VAP was determined with 5 mM p-nitrophenylphosphate in 1 M diethanolamine buffer containing 1.0 mM $MgCl_2$ at pH 9.8 and 25°C. The changes of absorbance were monitored at 405 nm.

2.6 Determination of kinetics

An approximately 5 mM nucleotide-phosphate solution was prepared and then serially diluted with the weakest concentration at 1/32th of the initial concentration. I used 0.1 M CAPS buffer with 1 mM $MgCl_2$ and 0.5 M NaCl at pH 9.8 for the nucleotide-phosphate solution and the protein solution. Three 700 µl samples of each nucleotide-phosphate concentration were put into three test tubes and then put into 25°C water. A 50 µl protein solution was then added to the solution and allowed to react with the substrates for 10 minutes in the case of ADP and ATP but 20 minutes for AMP because of low absorbance after 10 minutes. The absorbance was then plotted as a function of concentration. The data analysis software Kaleidagraph was used to determine K_m and V_{max} using the Michaelis-Menten equation.

k_{cat} was then deduced from V_{max} with the equation:

$$\mathbf{k_{cat}} = \frac{\mathbf{Vmax}\left(\frac{\mathbf{mM}}{\mathbf{min}}\right)}{[E]mM * \left(\frac{60sek}{\mathbf{min}}\right)} \qquad \mathbf{(9)}$$

2.7 Downloading AudoDock Vina

For docking, I choose the AutoDock Vina Software for Windows (the software is also available for Linux and MacOSX). It can be downloaded for free from

http://vina.scripps.edu/download.html

For running Autodock Vina, open the command prompt, find the folder in which Vina was installed and type:

"\Program Files\The Scripps Research Institute\Vina\vina.exe" –help

"\Program Files\The Scripps Research Institute\Vina\ being the default location.

For gridding (see section 2.9) and other purposes, Autodock tools must also be installed. AutoDockTools can be downloaded from: autodock.scripps.edu.

2.8 Downloading protein coordinate files for docking with Vina

PDB files from proteins can be accessed via the RCSB database:

http://www.rcsb.org/pdb/home/home.do

PDB files for ligands can be downloaded from:

http://ligand-expo.rcsb.org/

2.9 Docking

AutoDock Tools is first opened.

The next step is to import the structures. Either directly from the web by choosing file -> import Fetch from web and then enter the PDB code or open already downloaded and saved pdb file.

Figure 6 below shows the user interface of AutoDock tools. The protein structure can be seen inside the black window on the right.

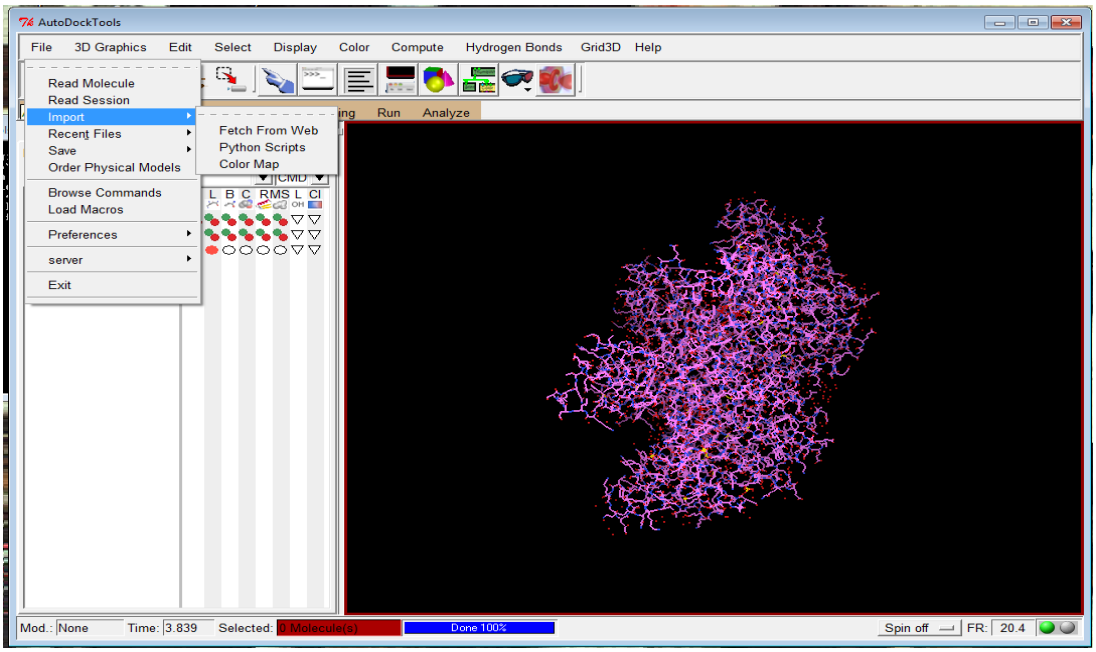

Figure 6: AutoDock tools interface. The protein structure can be seen inside the black window on the right. To import structures, press file -> import -> fetch from web.

Since most PDB structures do not include hydrogens, they must be added (Edit -> Hydrogens->ADD-> polar only).

In order to find the active site for alkaline phosphatase, I colored the atoms (Edit-> color patterns-> by Atom type) and colored the metal atoms red while the other prominent atoms (C, N, O, H) were colored yellow. This is done to increase the precision (preferably one should search within the volume of 27000 Ångström).

Figure 7 shows how to add hydrogens after the add button has been selected, select polar only.

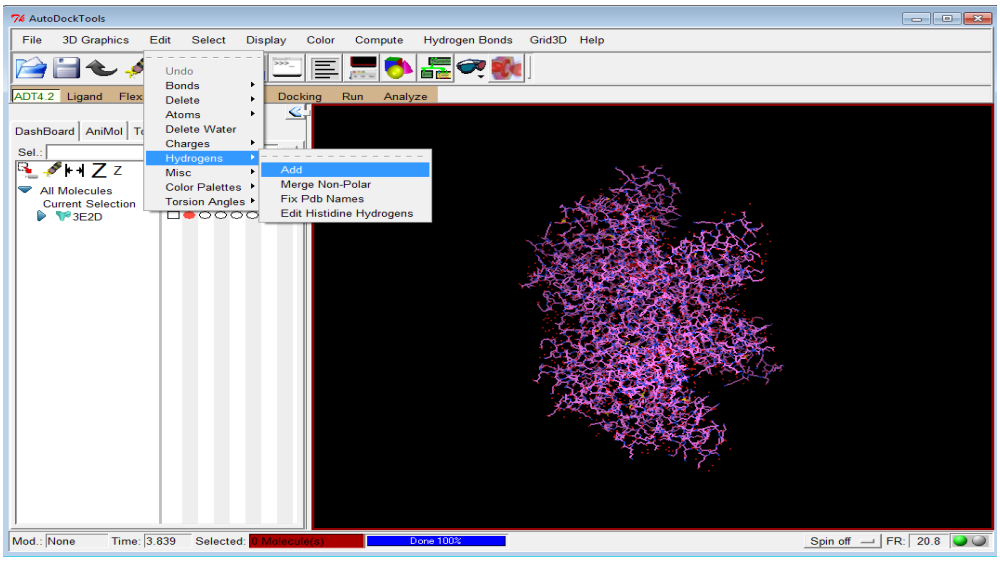

Figure 7: AutoDock tools interface. To add hydrogen, press: Edit -> Hydrogens->Add.

Then a pdbqt file is created by clicking Grid->Macromolecule-> choose and then save the file in the Vina Folder.

Figure 8 on the page below shows how to choose your macromolecule for gridding. The gridding is a vital step since it determines the coordinates suitable for docking.

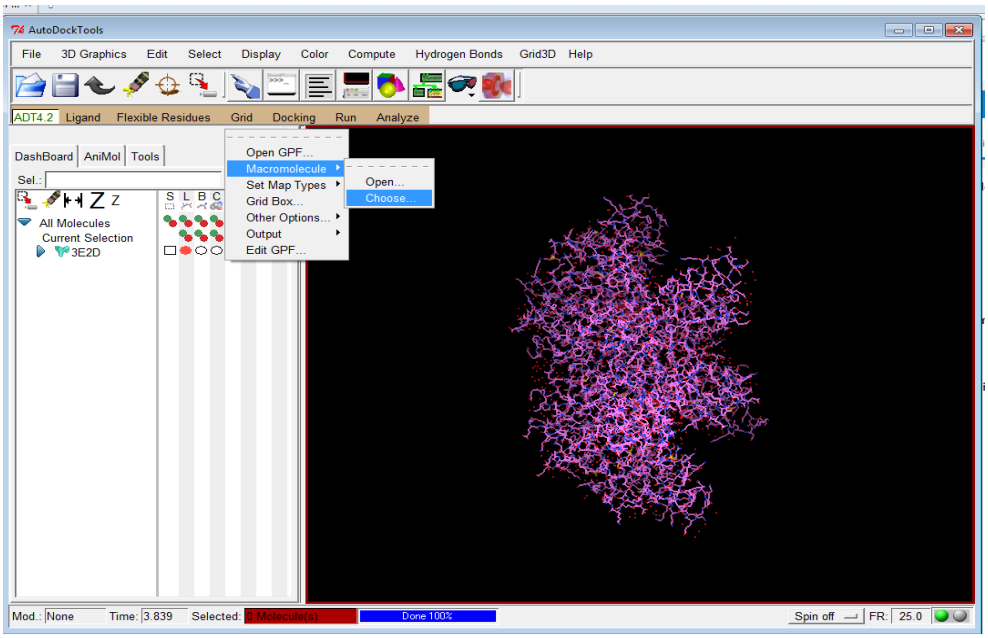

Figure 8: AutoDock tools interface. To choose macromolecule for gridding, press Grid-> Macromolecule -> choose.

Then a suitable position for the grid box must be determined. Click Grid-> Grid Box.

With the grid option window it is possible to select suitable coordinates for the center and size for the box. The volume of the grid box should preferably be less than 27000 $Å^3$. To make certain that the volume isn‘t larger than 27000 $Å^3$ the spacing should be 1.000 Ångström.

Figure 9 shows how gridding coordinates are selected. The box encompassing the protein’s active site is the grid box. The coordinates and the size of the grid box should be saved since they are used for the config file.

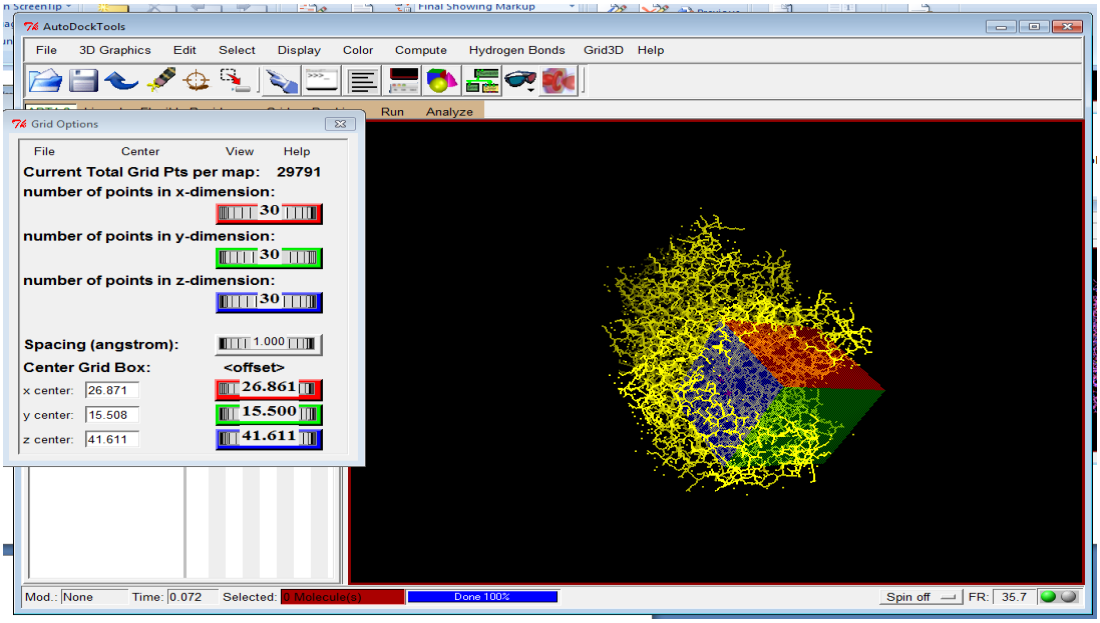

Figure 9: AutoDock tools interface. The box encompassing the protein’s active site is the grid box. The size of the box (preferably under 27000 $Å^3$) and the coordinates of the center of the box are adjusted by turning the buttons inside the Grad Options window on the left.

The next step is to find the ligand file. The ligand cannot be imported directly from the internet.

The ligand pdb file can be downloaded from the database: http://ligand-expo.rcsb.org/.

Figure 10 below shows how the ligand is imported. Unlike the protein structure it cannot be imported directly from the internet.

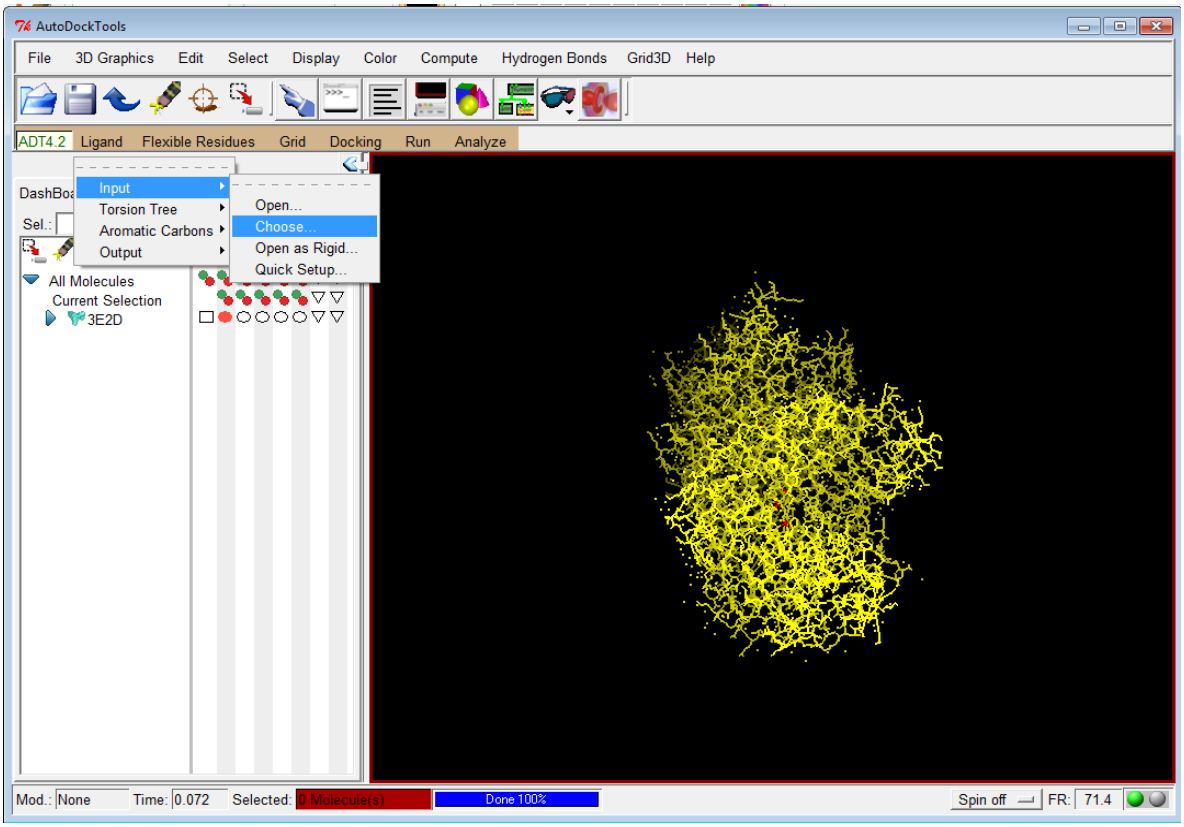

Figure 10: AutoDock tools interface. To import ligand file, press Ligand-> input->choose.

Then click Ligand->output and save the ligand file.

The final step before docking is to create a config text file as shown below on figure 11.

```
receptor = 3E2D.pdbqt    //protin file
ligand = ATP_ideal.pdbqt  // ligand file

out = out.pdbqt  //output  file

center_x = -2.111   // center of grid box
center_y = 20.472
center_z = 44.50

size_x = 30   // size of grid box
size_y = 30
size_z = 30

exhaustiveness = 10 // parameter which determines how thouroughly the
//Algorithm searches for optimal protin-ligand configuration.
```

Figure 11 shows how config file should be written. First the files used for the docking are specified then the center and finally the size of the box. Exhaustiveness level is by default 8 but it can be changed.

Finally, the actual docking takes place.

Vina is executed via the command prompt (see below).

Vina.exe –-config conf.txt –log log10.txt

Conf is the name of the configuration file (see above) while log is the name of the Log file which is automatically created after the running of AutoDockVina.

Figure 12 shows how AutoDockVina is run. First find the directory of the .exe file

and then write the command >vina.exe –config conf.txt –log log.txt

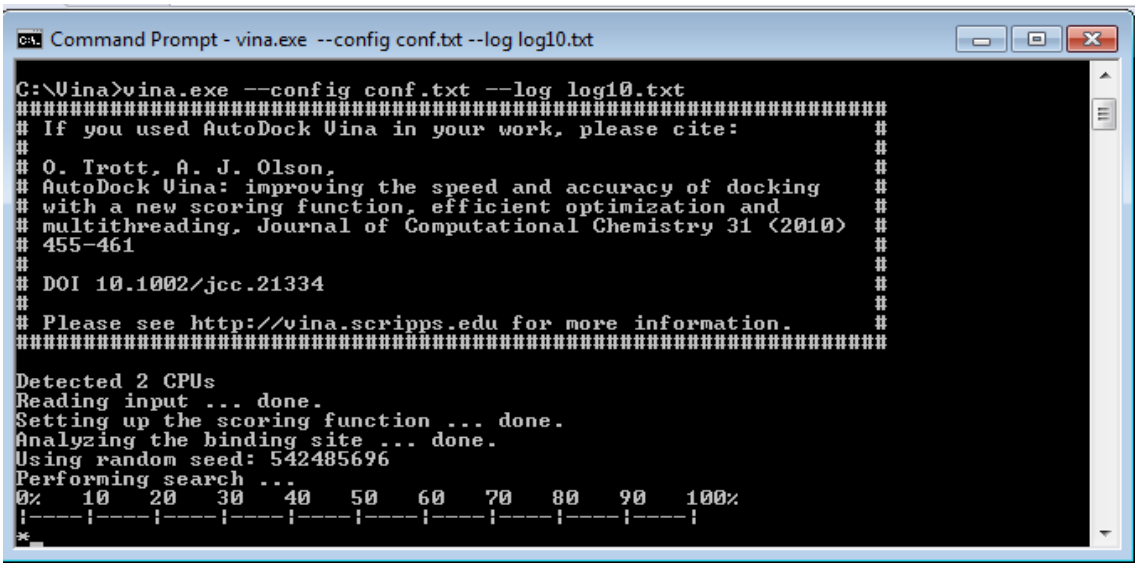

Figure 12: The commands necessary to run AutoDockVina are shown.

3. Results.

3.1 Determination of k_{cat} and K_m for AMP, ADP and ATP with VAP and ECAP

The concentration of inorganic phosphate after the reaction of enzyme and substrate was used to determine the Michaelis-Menten curve of the *Vibrio* and *E. coli* alkaline phosphatase with three substrates. The Rousers method was applied which involves using molybdate for concentration determination[30].

Tables 1-6 show the kinetics of the two proteins reacting with the three substrates. V_{max} was calculated from the Michaelis-Menten curves of the reactions using the software Kaleidagraph. The measurements were conducted at 25°C in a 0.1 M CAPS buffer with 1 mM $MgCl_2$ 0.5 NaCl and a pH of 9.8.

Table 1*:* V_{max} and K_m value for each Michaelis- Menten curve when VAP is the protein and AMP its substrate. V_{max} was calculated by using values from absorbance measurements at 625 nm. The errors for the fit were calculated with Kaleidagraph.

No. experiment	V_{max} (Absorbance/min)	K_m (mM)
1	0.093∓0.006	0.51∓0.08
2	0.090∓0.006	0.71∓0.17
3	0.087∓0.003	0.41∓0.06
Average	0.090∓0.003	0.54 ∓0.15

Table 2*:* **V_{max} and K_m values for each Michaelis-Menten curve when VAP is the protein and ATP its substrate. V_{max} was calculated by using values from absorbance measurements at 625 nm. The errors for the fit were calculated with Kaleidagraph.**

No. experiment	V_{max} (Absorbance/min)	K_m (mM)
1	0.095∓0.005	0.16∓0.03
2	0.103∓0.005	0.15∓0.04
3	0.093∓0.002	0.22∓0.03
Average	0.097∓0.005	0.18∓0.04

Table 3*:* **V_{max} and K_m values for each Michaelis -Menten curve when VAP is the protein and ADP its substrate. V_{max} was calculated by using values from absorbance measurements at 625 nm. The errors for the fit were calculated with Kaleidagraph.**

No. experiment	V_{max} (Absorbance/min)	K_m (mM)
1	0.12∓0.01	0.26∓0.06
2	0.11∓0.01	0.20∓0.07
3	0.08∓0.01	0.37∓0.14
Average	0.10∓0.02	0.28∓0.9

Table 4*:* V_{max} and K_m values for each Michaelis-Menten curve when ECAP is the protein and AMP its substrate. V_{max} was calculated by using values from absorbance measurements at 625 nm. The errors for the fit were calculated with Kaleidagraph.

No. experiment	V_{max} (Absorbance/min)	K_m (mM)
1	0.44∓0.01	0.100∓0.70
2	0.43∓0.03	0.120∓0.25
3	0.40∓0.01	0.071∓0.06
Average	0.42∓0.03	0.097∓0.03

Table 5*:* V_{max} and K_m values for each Michaelis-Menten curve when ECAP is the protein and ADP its substrate. V_{max} was calculated by using values from absorbance measurements at 625 nm. The errors for the fit were calculated with Kaleidagraph.

No. experiment	V_{max} (Absorbance/min)	K_m (mM)
1	0.36∓0.01	0.99∓0.08
2	0.41∓0.09	1.45∓0.61
3	0.31∓0.03	1.07∓0.26
Average	0.36 ∓0.05	1.17∓0.25

Table 6: V_{max} and K_m values for each Michaelis-Menten curve when ECAP is the protein and ATP its substrate. V_{max} was calculated by using values from absorbance measurements at 625 nm. The errors for the fit were calculated with Kaleidagraph.

No.experiment	V_{max} (Absorbance/min)	K_m (mM)
1	0.17∓0.02	0.35∓0.08
2	0.17∓0.01	0.56∓0.09
3	0.17∓0.02	0.72∓0.19
Average	0.17∓0.00	0.54∓0.19

Tables 7 and 8 below show the turnover number, K_m (mM) and k_{cat} /K_m ($s^{-1}mM^{-1}$) of the three substrates for VAP and ECAP at 25 °C in 0.1 M CAPS buffer containing 1 mM $MgCl_2$ and 0.5 NaCl at pH 9.8.

Table 7: VAP's kinetic values of k_{cat}, K_m and k_{cat}/K_m for each of the substrates AMP, ADP and ATP. The values were deduced from phosphate concentration after reaction at 25 °C* in *0.1 M CAPS* buffer *containing1 mM $MgCl_2$ and 0.5 NaCl with pH of 9.8 for 10-20 minutes. The error represents the standard deviation of n=3.

Substrate	**k_{cat} (s^{-1})**	**K_m (mM)**	**k_{cat} /K_m ($s^{-1}mM^{-1}$)**
AMP	3.94±0.36	0.54±0.15	7.3±2.1
ADP	9.46±0.68	0.28±0.09	33.8±11.3
ATP	10.28±0.64	0.18±0.04	57.1±13.2

Table 8: ECAP's kinetic values of k_{cat}, K_m and k_{cat}/K_m for each of the substrates AMP, ADP and ATP. The values were deduced from phosphate concentration after reaction at 25°C* in *0.1 M CAPS buffer containing 1 mM $MgCl_2$ and 0.5 NaCl with pH of 9.8 for 10-20 minutes. The error represents the standard deviation of n=3.

Substrate	**k_{cat} (s^{-1})**	**K_m (mM)**	**k_{cat}/K_m ($s^{-1}mM^{-1}$)**
AMP	4.00±0.09	0.97±0.3	4.1±1.3
ADP	6.82±0.52	1.17±0.25	5.8±1.3
ATP	3.00±0.44	0.54±0.19	5.6±2.1

3.2 Results from docking.

3.2.1 The big picture

The three substrates, AMP, ADP and ATP, were docked with Autodock Vina into *VAP* and *ECAP* respectively. The results can be seen in figures 13-15 below. Overall free energy results from all the possible conformations can be seen in tables 11-16 in Appendix E.

Figure 13 below shows how ATP fits into the active sites of VAP (on the right) and ECAP (on the left) at pH 9.8. The color of the surface represents the electrostatic forces. Red represents negative electrostatic surface, white represents neutral surface while blue represents positive electrostatic surface.

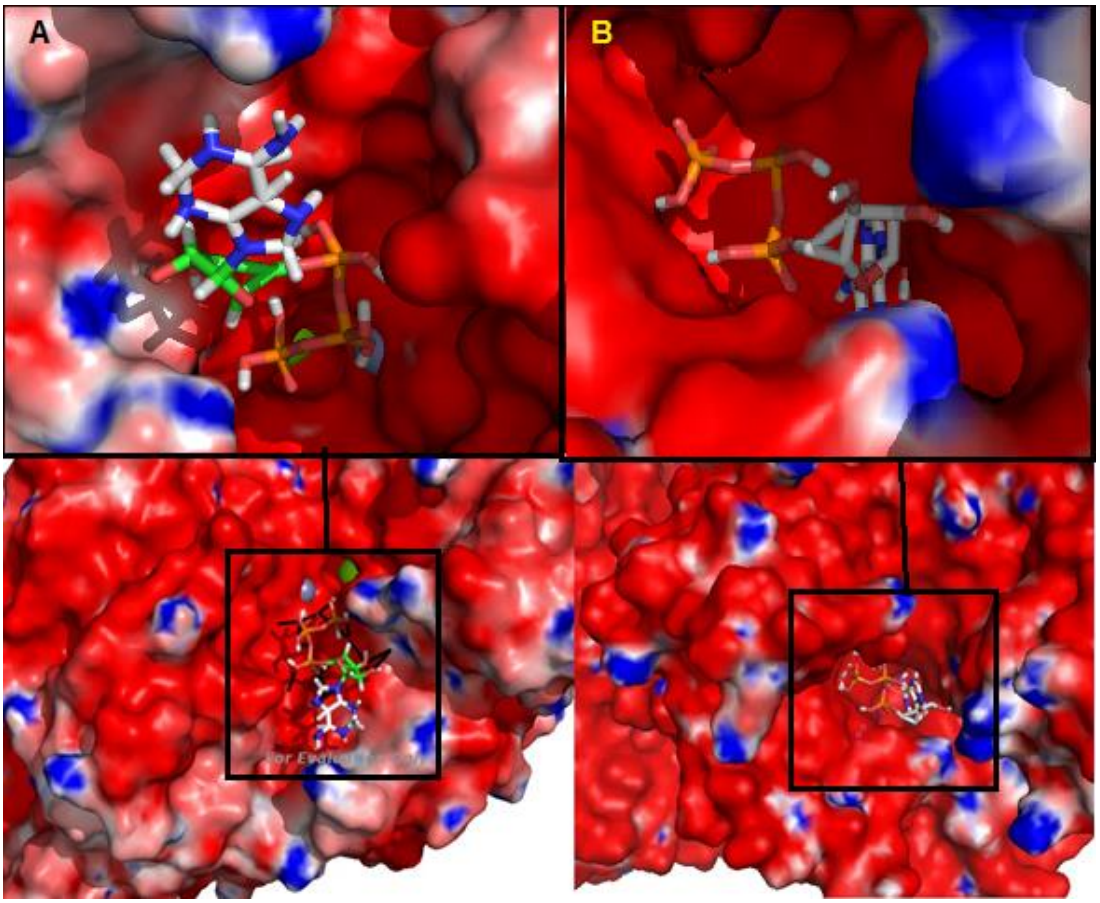

Figure 13: The binding of the ligand ATP inside the proteins' active site. VAP's pocket (B) seems to be deeper than ECAP's pocket (A). The upper figure shows the substrate inside the enzymes' pocked while the lower figure shows the big picture. There is a clear difference between the configurations of the substrates as the terminal phosphate of ATP turns more inwards in ECAP's case and closer to the metal ions. The grey sphere represents one of two zinc ions found in ECAP and the green sphere represents magnesium. The figure was made in the application PyMol.

Figure 14 shows the difference between how ADP fits into the active sites of VAP (on the right) and ECAP (on the left) at pH 9.8. The color of the surface represents the electrostatic surface. Red represents negative electrostatic surface, white represents neutral surface while blue represents positive electrostatic surface.

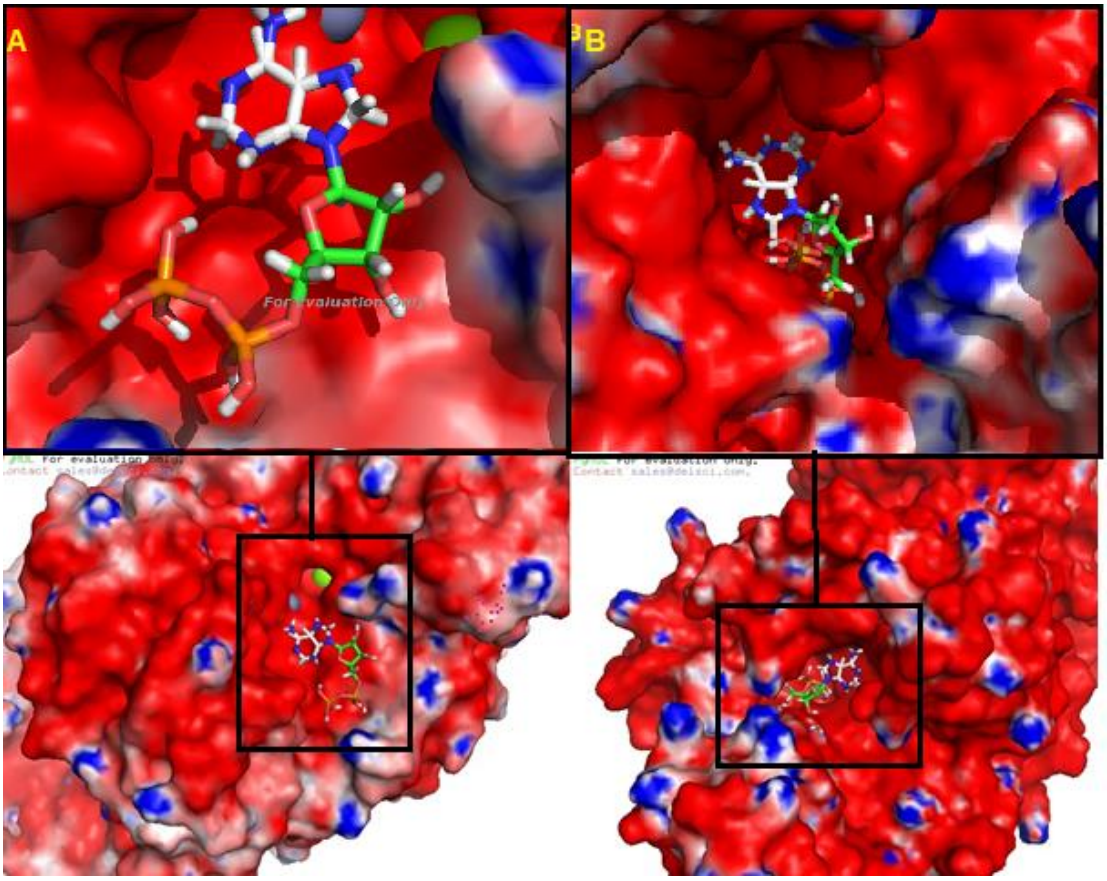

Figure 14: Binding of the ligand ADP inside the proteins' active site. VAP's pocket (B) seems to be deeper than ECAP's (A). The upper figure shows the substrate inside the enzymes' pocked while the lower figure shows the big picture. The most striking difference between ADPs conformation is that the phosphate tail of ADP in VAP turns inwards while it turns outwards (away from metal ions) inside ECAP's active site. In both cases it is the opposite with bound ATP. The grey sphere represents one of two zinc ions found in ECAP and the green sphere represents the Mg ion. The metal ions are closer to the surface in ECAP's active and are therefore visible on this figure. The figure was made in the application PyMol.

Figure 15 on next page shows how AMP fits into the active sites of VAP (on the right) versus the active site of ECAP (on the left) at pH 9.8. The color of the surface represents electrostatic forces. Red represents negative electrostatic surface, white represents neutral surface while blue represents positive electrostatic surface.

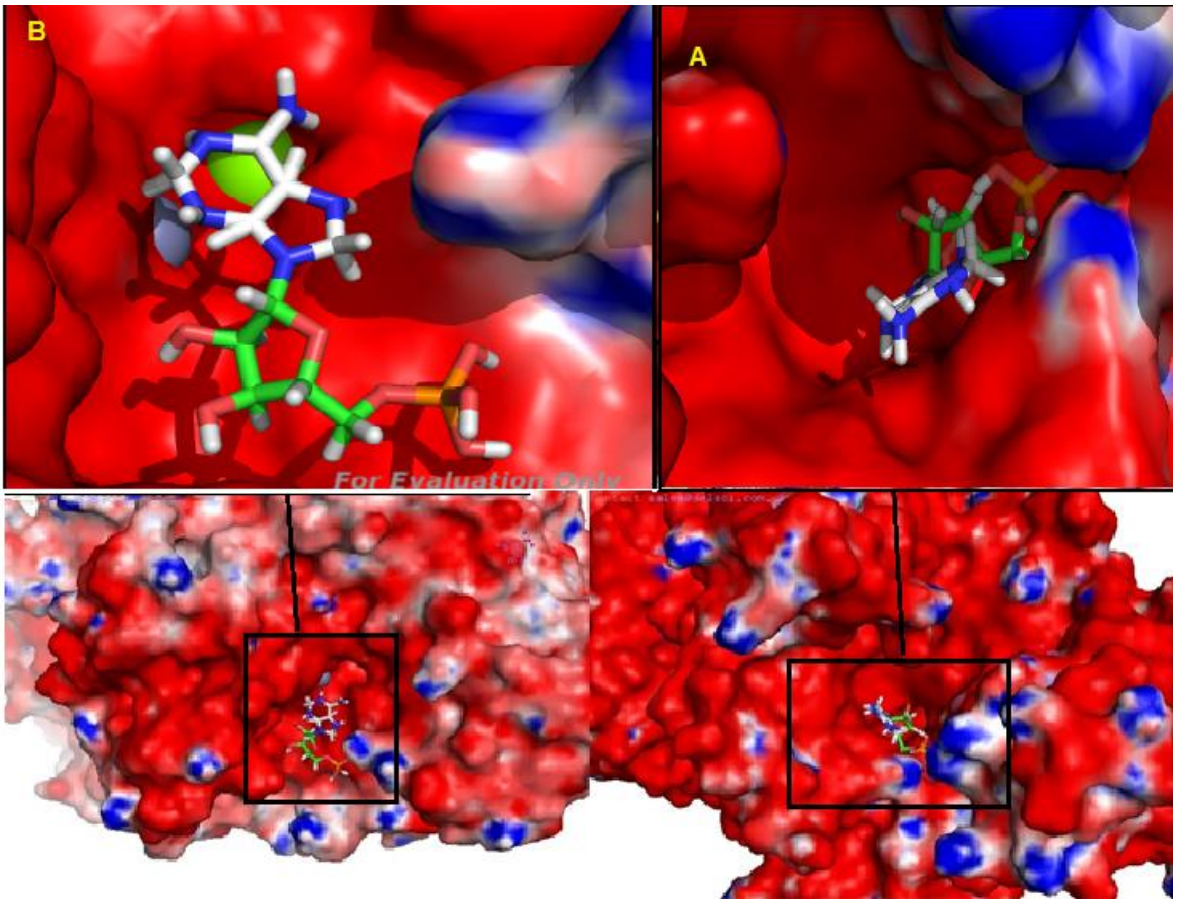

Figure 15: Binding of the ligand AMP inside the proteins' active site. The VAP's pocket (A) seems to be deeper than ECAP's (B). The upper figure shows the substrate inside the enzymes' pocked while the lower figure shows the big picture. The most striking difference between AMPs conformation is that the phosphate tail of AMP in VAP turns inwards while it turns outwards (away from metal ions) inside ECAP's active site The grey sphere represents one of two zinc ions found in ECAP and the green sphere represents the only mg ion. The magnesium ion is closer to the surface in ECAP's active and is therefore visible on this figure. The figure was made in the application PyMol.

3.2.2 Conformation of ligand inside the active sites of aligned proteins.

The ligands 3-D conformation inside the active sites of VAP and ECAP were attained by docking with AutoDock Vina. The conformations below (figures 16-

18) show the conformations of AMP, ADP and ATP inside the active sites of ECAP and VAP which have the lowest free energy.

Figure 16 below shows the docking conformation with the lowest calculated free energy of ADP when docked into *ECAP's* active site (to the left) and *VAP's* active site (to the right) at pH 9.8 after the two proteins have been aligned using *PyMol.* The orientations were clearly very different and the terminal phosphates not in the equivalent position although the bond that is cleaved should be in similar proximity to the catalytic serines.

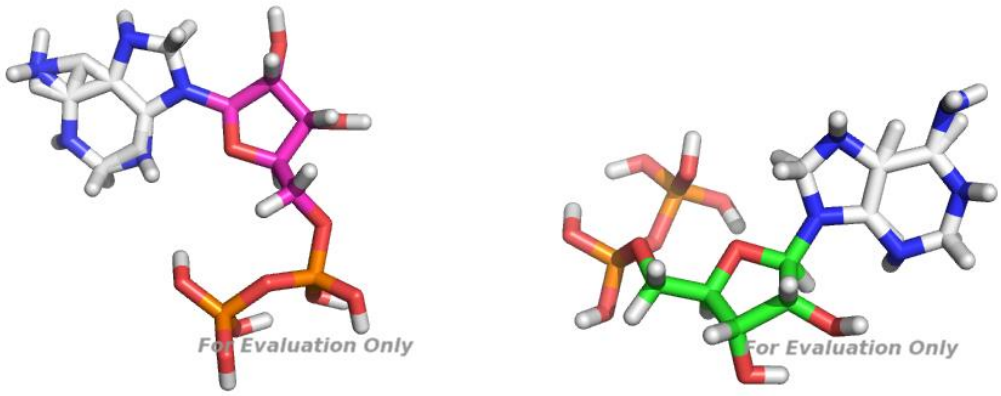

Figure 16: The most energetically stable conformations of ADP according to Autodock Vina. The conformation on the right represents the conformation of ADP in VAP's active site and the conformation on the left represents ADP inside the active side of ECAP. The free energy conformation scoring was -8 kJ/mol for VAP and -5.7 kJ/mol for ECAP. The figure was made in the application PyMol.

Figure 17 shows the energetically most stable conformation of AMP inside the active sites of *VAP* on the right and *ECAP* on the left according to AutoDockVina at pH 9.8 after the two proteins have been aligned using PyMol.

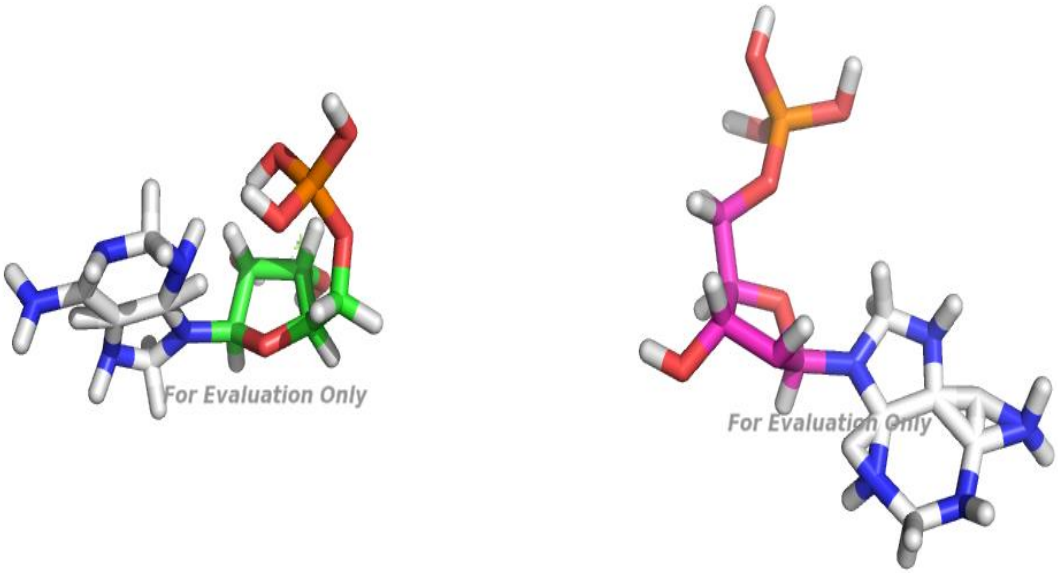

Figure 17: The conformations with the lowest calculated free energy when AMP is docked into ECAP's active site (to the left) and VAP's active site (to the right) after the two proteins have been aligned using PyMol. The free energy of the most suitable conformation according to the scoring was -7.8kJ/mol for VAP and -4.9 kJ/mol for ECAP. The orientation of the substrates is strikingly different given how related the enzymes are. The figure was made in the application PyMol.

Figure 18 shows the energetically most stable conformation of ATP inside the active sites of *VAP* on the right and *ECAP* on the left according to AutoDock Vina at pH 9.8 after the two proteins have been aligned using PyMol. Again the conformations and the binding free energy were very different but in this case the terminal phosphates falls within similar proximity to the metal ions found inside the enzymes' active sites.

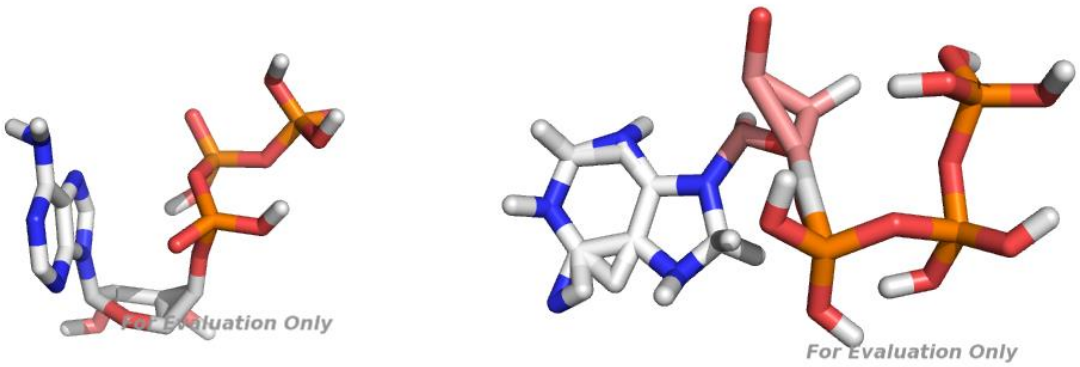

Figure 18: The conformations with the lowest calculated free energy when ATP is docked into ECAP (left) and VAP (right) after the two proteins have been aligned using PyMol. The free energy of the most suitable conformation according to the scoring was -8.1 *kJ/mol for VAP and -1.8 kJ/mol for ECAP. The conformations of the substrates are quite different but in ATP's case the terminal phosphate falls within similar proximity to the metal ions inside the enzymes' pocket. The figure was made in the application PyMol.*

As figures 13-18 show that the conformations of lowest free energy vary between enzymes (VAP or ECAP) in the cases of ATP, AMP and ADP. However, the terminal phosphate of ATP is in similar location inside the active sites of VAP and ECAP. The terminal phosphates of AMP and ADP are however, not within the same proximity nor do they have similar orientation.
Table 9 shows the calculated free energy of enzyme-substrate complexes. The values were calculated using AutoDockVina docking software.

Table 9: The free energies of the enzyme-substrate complexes. The free energy values were calculated using AutoDockVina docking software.

substrate	ΔG of ECAP+substrate (kJ/mol)	ΔG of VAP+substrate (kJ/mol)
AMP	-4.9	-7.8
ADP	-5.7	-8.0
ATP	-1.8	-8.1

In all cases there is a considerable difference between the free energies of ECAP-substrate complexes and VAP-substrate complexes (table 9). The conformations were quite different. The terminal phosphates of AMP and ADP turned outwards relative to the metal ions. However, AMP and ADP do have other possible conformations (see tables 14 and 15) which might be more suitable in practice.

3.2.3 Ligands and hydrogen bonds.

On the figures below (19-21) the hydrogen bonds which are formed between the ligand and the protein are represented with black dotted lines. The amino acids are represented with shortened version of their names and a number representing their position in the amino acid chain. Water molecules are represented as white (hydrogen) and red (oxygen) atoms. Figure 19 compares both the number and positions of hydrogen bonds which AMP forms with the alkaline phosphatases when AMP is in the configuration with the lowest free energy.

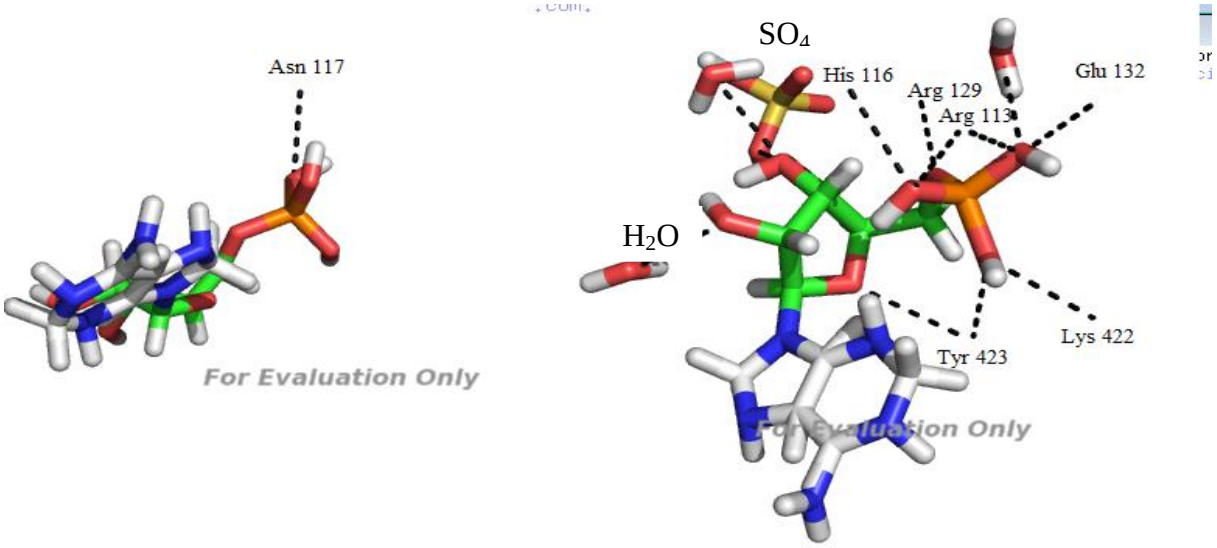

Figure 19: AMP in ECAP's (on the left) and in VAP's active site. The black dotted lines represent hydrogen bonds. The figure shows that AMP forms more hydrogen bonds with VAP than ECAP since AMP only forms one hydrogen bond with ECAP it forms 8 hydrogen bonds with amino acids within the VAP structure and 3 with water molecules found inside the active site and one with SO_4*. This means that the VAP should have more affinity towards AMP than ECAP. Water molecules are represented as red (oxygen) and white (hydrogen) molecules. The figure was made in the application PyMol.*

Figure 20 compares both the number and positions of hydrogen bonds which ADP forms with the alkaline phosphatases when ADP is in the configuration with the lowest free energy. Once again, the substrate (ADP) forms more hydrogen bonds with VAP (6) compared to the number of hydrogen bonds formed with ECAP (2).

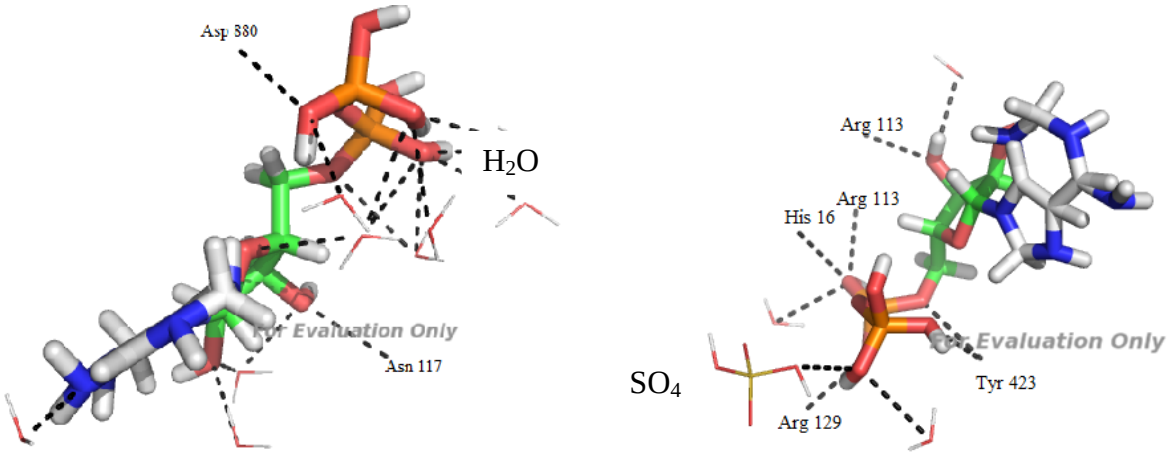

Figure 20: ADP in ECAP's (on the left) and VAP's active site. The black dotted lines represent hydrogen bonds. ADP in ECAP's active site forms 16 hydrogen but most of them (14) are formed with water molecules inside the active site or at the surface of the protein. ADP forms 10 hydrogen bonds inside VAP's active site thereof 3 are formed with water, one with SO_4 and six with amino acids found within the VAP structure. This means that the VAP should have more affinity towards AMP than ECAP. Water molecules are represented as red (oxygen) and white (hydrogen) molecules. The figure was made in the application PyMol.

Lastly, the number of hydrogen bonds ATP formed with its surroundings inside ECAP's and VAP's active site (figure 21) were compared. ATP formed more hydrogen bonds with amino acids in VAP's active site than it did in ECAP's (5 vs 1). ATP formed 6 hydrogen bonds with water molecules and one with SO_4 inside VAP's active site while it formed 15 hydrogen bonds with water in ECAP's active site.

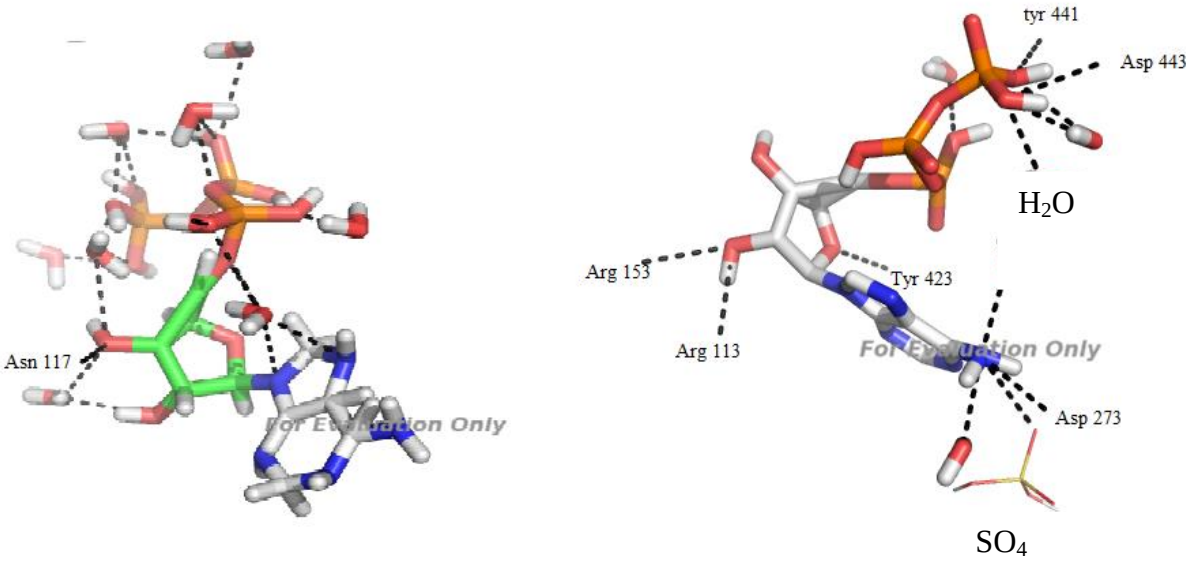

Figure 21: ATP in ECAP's (on the left) and VAP's active site. The black dotted lines represent hydrogen bonds. Only one hydrogen bond is formed between ECAP and ATP the other 16 are formed with water molecules. VAP on the other hand forms 6 hydrogen bonds with ATP while 6 hydrogen bonds are formed between ATP and water. This means that the VAP should have more affinity towards AMP than ECAP. Water molecules are represented as red (oxygen) and white (hydrogen) molecules. The figure was made in the application PyMol.

Table 10 provides overview over the number of hydrogen bonds formed within each enzyme-substrate complex. These numbers were provided with PyMol molecular modeling software when the substrates AMP, ADP and ATP were in the most free energetically stable conformation. Therefore, in some cases there might be possible conformations with more hydrogen bonds but more positive free energy.

Table 10: Number of hydrogen bonds each substrate forms in the active sites of ECAP and VAP according to PyMol.

Enzyme-substrate complex	Number of hydrogen bonds with enzyme	Numberof hydrogen bonds with water	Number of hydrogen bonds with SO_4	total
VAP+AMP	8	3	1	12
ECAP+ AMP	1	0	0	1
VAP+ADP	6	3	1	10
ECAP+ ADP	2	14	0	16
VAP+ATP	6	6	1	13
ECAP+ ATP	*1*	16	0	17

Overall, more hydrogen bonds were formed between the substrates and VAP compared to ECAP. VAP had lower K_m for all substrates (ATP, ADP and AMP) compared to the K_m value of ECAP for each substrate.

4. Conclusion

Overall, I was not able to reproduce the research conducted by Guðrún Jónsdóttir and Bjarni Ásgeirsson, namely that VAP did not manage to catalyze the dephosphorylation of ADP and ATP[31]. However, my data is consistent with Kaufman's and Graßmann's results when the activity of intestinal alkaline phosphatase towards AMP, ATP and ADP was investigated (see figure 4). Their results showed that alkaline phosphatase from human intestines had higher activity towards ATP and ADP compared to AMP [20] which is consistent with my results regarding VAP.

Earlier, in a study conducted in 1980, Karl and Craven found out that *E. coli* alkaline phosphatase was able to hydrolyze AMP, ADP and ATP but according to their findings AMP was the preferred substrate[32] which does not fit my findings where ADP was the preferred substrate. However, according to my results ECAP had lower activity towards ATP than AMP.

According to my results, ECAP had lower activity towards ATP and ADP compared to VAP as was to be expected since VAP is among the most active alkaline phosphatases and its adaptation to cold environments should render its active site more flexible. It is, however, inconclusive which enzyme is more active towards AMP since the difference is only 0.03 s^{-1} which falls well within the calculated error. The small size of the AMP might explain the difference as AMP can easily access ECAP's active site even though binding into ECAP's active site is more free energy demanding than binding into VAP's active site. In all cases, VAP had lower K_m values but the difference was more pronounced between AMP and ATP. The lower K_m values are surprising since k_{cat} /K_m are usually similar independent of environmental adaption with natural substrates[33]. This attribute of the *Vibrio* alkaline phosphatase is probably due to other factors than cold adaption alone. According to my results all three substrates formed more hydrogen bonds with VAP so that might at least partly explain the difference.

The docking results partly support these results as the free binding energy was negative in all cases but more so in the case of VAP. When the nucleotides were

docked into VAP ADP and ATP had more negative binding energies compared to the energy of AMP but when docked into ECAP, ATP had a binding energy closer to zero than that of AMP while ADP‘s binding energy was the most negative. Also it is worthy to mention, that in all cases the phosphate group of the substrate entered the active site of VAP more deeply. In ECAP, this difference was more pronounced in the case of ADP and AMP where the configurations with the lowest energy led the phosphate groups to turn away from the metal ions found in the active site.

The method used in this project to measure phosphate concentration (described in chapter 2.1) turned out to be able to consistently measure the concentration. The method, however, is rather complex to use due to extraction with organic solvents. This method was chosen since using the Biomol Green had not turned out well in other experiments[31,30].

Alkaline phosphatases have many practical roles in research. Currently alkaline phosphatases are being used to cleave nucleoside –phosphates for purposes such as PCR to treat unincorporated dNTP for DNA sequencing. Usually, shrimp alkaline phosphatase has been used for this purpose as it can easily be irreversibly deactivated with heating at 65 °C for 15 minutes[34]. However, according to my results VAP might be used for this purpose as well, as it is active towards ATP and its cold-adaption and high activity means that it is in many ways similar to the shrimp alkaline phosphatase. ECAP on the other hand is not as suitable for PCR.

In the future, it would be interesting to experiment with other substrates such as other nucleotides and sugar phosphates such as α and β –glycerophosphate and compare the activity of the two phosphatases towards those substrates. Another interesting possibility would be to mutate certain amino acids inside the active sites of VAP and ECAP to find out what causes the difference between the two enzymes, the main difference being that VAP has the highest activity towards ATP of the three nucleotides while ECAP has the lowest.

Borgþór Pétursson, 10. July 2014

References:

1. O'Brien, P.J. & Herschlag, D. Catalytic promiscuity and the volution of new enzymatic activities. *Chem Biol.* **6**, 91-105 (1999).
2. Khersonsky, O. & Tawfik, D.S. Enzyme Promiscuity: A Mechanistic and Evolutionary perspective. in *Ann Rev Biochem.* **79** 471-505 (2010).
3. WF, Li., XX, Zhou. & P, Lu. Structural features of thermozymes. *Biotechnol Adv.* **23**, 271-281 (2005).
4. C., Vieille. & GJ, Zeilkus. Hyperthermophilic enzymes: sources, uses, and molecular mechanisms for thermostability. *Microbiol Mol Biol Rev.* **65**, 1-43 (2001).
5. Feller, G. & Gerday, C. Psychrophilic Enzymes: Hot topics in cold adaption. *Nat Rev Microbiol.* **1**, 200-208 (2003).
6. Elias, M., Wieczorek, G., Rosenne, S. & Tawfik, D.S. The universality of enzymatic rate-temperature dependency. *Trends Biochem Sci.* **39**, 1-7 (2014).
7. Nelson, D.L. & Cox, M.M. *Lehninger Principles of Biochemistry*, (W.H. Freeman and Company, New York, 2008).
8. Ásgeirsson, B. & Andrésson, Ó.S. Primary structure of cold -adapted alkaline phosphatase from *Vibrio* sp. as deduced from the nucleotide gene sequence. *Biochim Biophys Acta***1549**., 99-111 (2001).
9. Kim, E.E. & Wyckoff, H.W. Reaction mechanism of alkaline phosphatase based on crystal structures. Two-metal ion catalysis. *J Mol Biol.* **218**, 449-469 (1991).
10. Millán, J.L. Alkaline phosphatase as a reporter of cancerous transformation. *Clin Chim Acta* **209**, 123-129 (1992).
11. Murphy, J.E., Tibbitts, T.T. & Kantrowitz, E.R. Mutations at positions 153 and 328 in *Escherichia coli* alkaline phosphatase provide insight towards the structure and function of mammalian and yeast alkaline phosphatases. *J Mol Biol.* **253**, 604-617 (1995).
12. Millán, J.L. Alkaline phosphatases: Structure, substrate specificty and functional raletedness to other memepers of a large superfamily of enzymes. *Purinergic Signal.***2**, 335-341 (2005).

13. Helland, R., Larsen, R. & Ásgeirsson, B. 1.4 Å crystal structure of the large and cold-active *Vibrio* sp. alkaline phosphatase. *Biochim Biophys Acta* **1794,** 297-308 (2009).
14. Fernley, H.N. Thiophosphorylation of Alkaline Phosphatase. *Nat New Biol.* **241**, 110-111 (1973).
15. Tordo, D.C., Fosset, M., Iwatsubo, M., Gache, C. & Ladunski, M. Intestinal alkaline phosphatase. Catalytic properties and half of the sites reactivity. *Biochemistry* **13,** 1788-95 (1974).
16. Anderson, R.A., Bosron, W.F., Kennedy, F.S. & Vallee, B.L. Role of magnesium in *Escherichia coli* alkaline phosphatase. *Proc Natl Acad Sci U S A* **72**, 2989–2993. (1975).
17. Garen, A. & Levinthal, C. A fine-structure genetic and chemical study of the enzyme alkaline phosphatase of *E. coli* I. Purification and characterization of alkaline phosphatase. *Biochim Biophys Acta* **38**, 470-483 (1960).
18. Bock, J. & Sheard, B. ^{31}P NMR of Alkaline Phosphatase *Biochem Biophys Res Commun.* , 24-30 (1975).
19. B., S., Holtz, K.M. & Kantrowitz, E.R. A revised mechanism for the alkaline phosphatase reaction involving three metal ions. *J Mol Biol.* **299**, 1303-1311 (2000).
20. Kaufman, C.M., Graßmann, J., Treutter, D. & Letzel, T. Utilization of real time electrospray ionization mass spectrometry to gain further insight into the course of nucleotide degradation by intestinal alkaline phosphatase. *Rapid Commun, Mass Spectrom.* **28**, 869-878 (2014).
21. Malo, M.S. Alam SN, Mostafa G, Zeller SJ, Johnson PV, Mohammad N, Chen KT, Moss AK, Ramasamy S, Faruqui A, Hodin S, Malo PS,Ebrahimi F, Biswas B, Narisawa S, Millán JL, Warren HS, Kaplan JB, Kitts CL, Hohmann EL, Hodin RA.. Intestinal alkaline phosphatase preserves the normal homeostasis of gut mocribiota. *Gut.* **59**, 1476-1484 (2010).
22. Bik, E. Composition and function of the human associated microbiota. *Nutr Rev.* **67**, 164-171 (2009).
23. LV, Hooper. & JI, Gordon. Commensal host-bacteria relationships in the uts. *Science* **292,** 1115-1118 (2001).

24. II, Ivanov. & Honda K. Intestinal commensal microbes as immune modulators. *Cell host & microbe.* **12**, 496-508 (2012).
25. EG, Zoetendal., M, Rajilic-Stojanovic & WM., de Vos High-throughput diversity and functionality analysis of the gastrointestinal tract microbiota. *Gut.* ***57***, 1605-1615 (2008).
26. Malo, M.S., Moaven O,Muhammad N, Biswas B, Alam SN, Economopoulos KP, Gul SS, Hamarneh SR, Malo NS, Teshager A, Mohamed MM, Tao Q,Narisawa S, Millán JL, Hohmann EL, Warren HS, Robson SC, Hodin RA. Intestinal alkaline phosphatase promotes gut bacterial growth by reducing the concentration of luminal nucleotide triphosphates. *Am J Physiol* **10**, G826-838 (2014).
27. Lengauer, T. & Rarey, M. Computational methods for biomolecular docking. *Curr Opin Struct Biol.***6**, 402-407 (1996).
28. Trott, O. & Olson, A.J. AutoDock Vina: improving the speed and accuracy of docking with a new scoring function, efficient optimization and multithreading. *J Comput Chem..**31***, 455-461 (2010).
29. Heidarsson, P.O., Sigurdsson, S.T. & Ásgerisson, B. Structural features and dynamics of a cold-adapted alkaline phosphatase studied by EPR spectroscopy. *FEBS J.* **276**, 2725-2735 (2009).
30. Gylfason, G. A., Knútsdóttir, E., and Ásgeirsson, B. Þróun á aðferð við þáttun frumuhimnuhluta úr þarmaþekjufrumu Atlantshafsþorsks (Gadus morhua), *Sérrit Raunvísindastofnunar (Report Series of the Science Institute, University of Iceland) RH-20-08*, p. 33. (2008).
31. Ásgeirsson, B., and Jónsdóttir, G. Áhrif hindra og mismunandi hvarfefna á virkni alkalísks fosfatasa úr Vibrio sjávarörveru í samanburði við skyld ensím (Effects of inhibitors and different substrates on the activity of alkaline phopshatse from a Vibrio marine bacterium in comparison with related enzymes), *Sérrit Raunvísindastofnunar (Report Series of the Science Institute, University of Iceland) RH-19-08*, p. 49. (2008).
32. Karl, D.M. & Craven, D.B. Effects of Alkaline Phosphatase Activity on Nucleotide Measurements in Aquatic Microbial Communities. *Appl Environ Microbiol.* **40**, 549-561 (1980).

33. Georlette, D. Damien B, Blaise V, Depiereux E, Uversky VN, Gerday C, Feller G. Structural and functional adaptations to extreme temperatures in psychrophilic, mesophilic and thermophilic DNA ligases. *J Biol Chem.* **278**, 37015-37023 (2003).
34. Nilsen, I.W., Olsen, R.L. & Øverbø, K. Thermolabile alkaline phosphatase from Northern shrimp (Pandalus borealis): protein and cDNA sequence analyses. *Comp Biochem Physiol B Comp Biochem* **129**, 853-861 (2001).

APPENDIX A

Phosphate standard curve

For the determination of phosphate concentration, the phosphate standard curve which can be seen below was used.

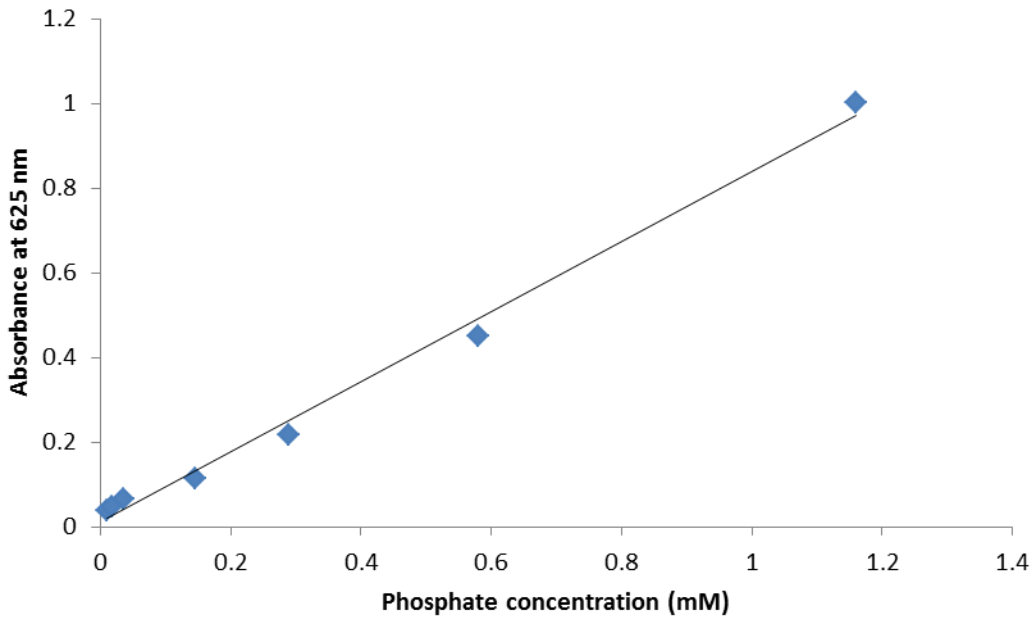

Figure 22: Phosphate concentration shown as a function of absorbance at 625 nm. The data follows the linear equation: y = 0.826x + 0.012

APPENDIX B

Protein concentration standard curve.

For the determination of protein concentration a standard curve was created using The Zaman and Verwilghen (1979) method.

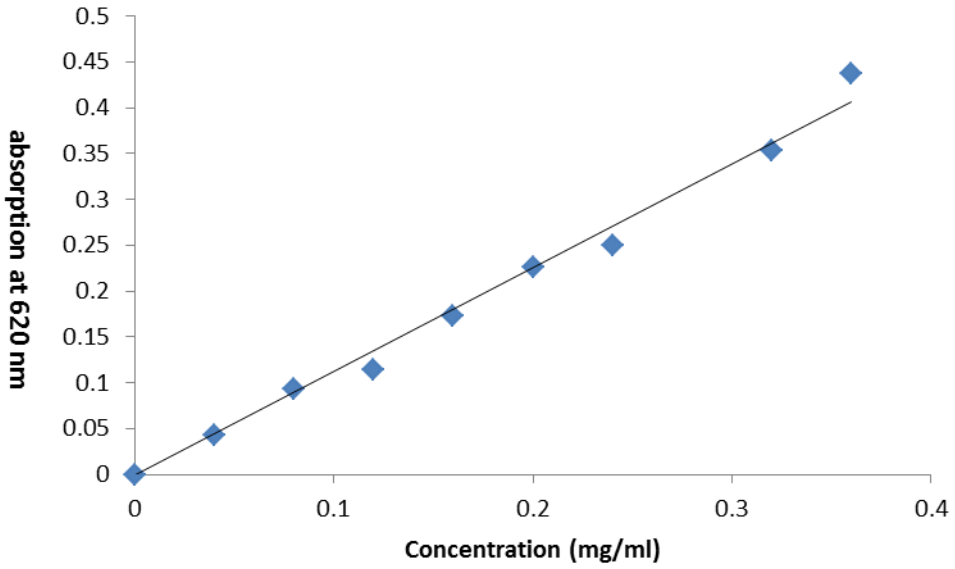

Figure 23: Protein concentration as a function of absorbance at 620 nm. The data follows the linear equation: y = 1.1272x.

APPENDIX C

Michaelis-Menten curves for VAP and ECAP

Figures 24 to 29 show the Michaelis-Menten curves for the substrates AMP, ATP and ADP.

Tables 3-5 show the V_{max} in absorption units and the K_m value for each substrate.

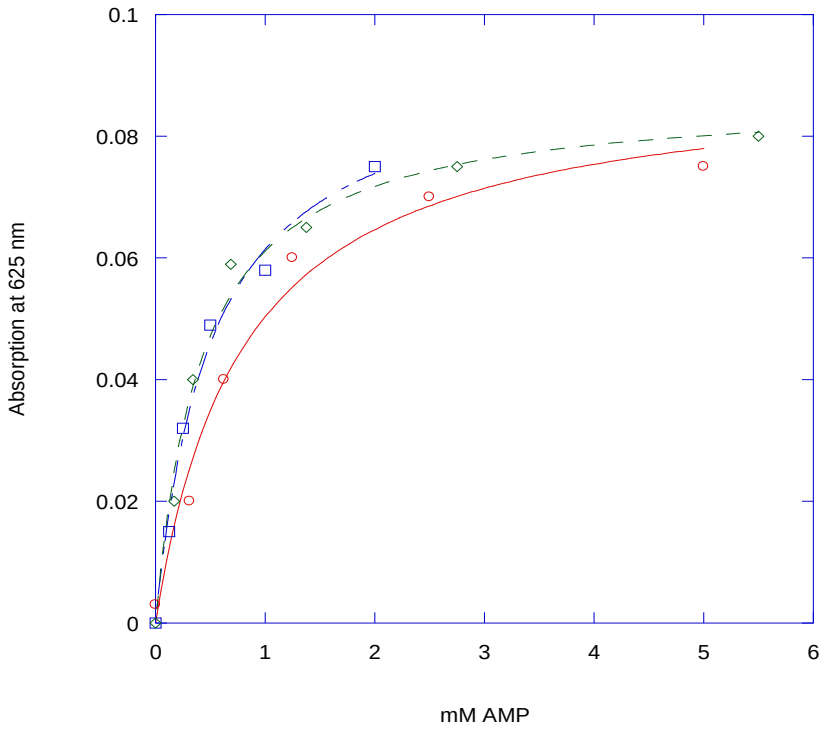

Figure 24: The Michaelis-Menten curve for VAP when AMP was the substrate. The concentration of AMP is plotted against the absorbance at 625 nm (indicative of phosphate concentration). These curves from independent experiments where used to determine the turnover number and K_m value. The measurements were conducted at pH 9.8 (0.1 M CAPS buffer with 1 mM $MgCl_2$ and 0.5 M NaCl at pH 9.8) and 25°C. VAP was allowed to react with AMP for 20 minutes.

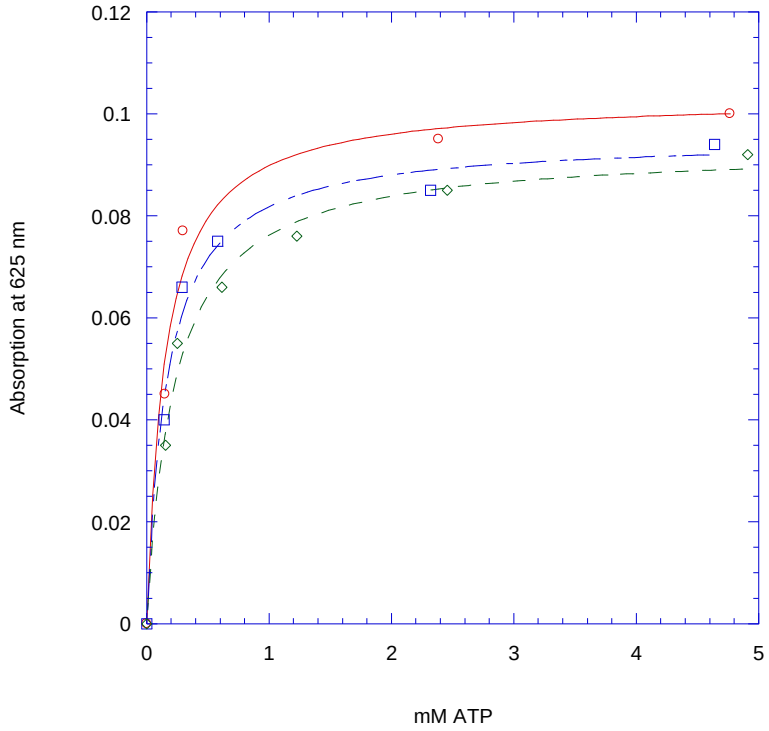

Figure 25: The Michaelis-Menten curve for VAP when ATP was the substrate. The concentration of ATP is plotted against the absorbance at 625 nm (indicative of phosphate concentration). These curves from independent experiments were used to determine the turnover number and K_m value. The measurements were conducted at pH 9.8 (0.1 M CAPS buffer with 1 mM $MgCl_2$ and 0.5 M NaCl at pH 9.8) and 25 °C. VAP was allowed to react with ATP for 10 minutes.

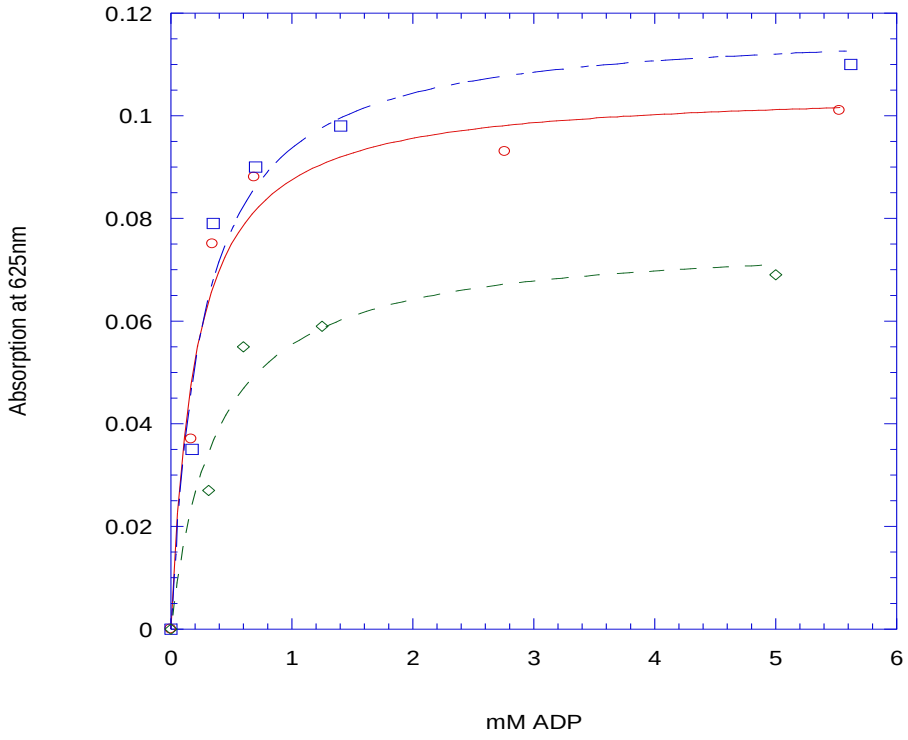

Figure 26: The Michaelis-Menten curve for VAP when ADP was the substrate. The concentration of ATP was plotted against the absorbance at 625 nm (indicative of phosphate concentration). These curves from independent experiments were used to determine the turnover number and K_m value. The measurements were conducted at pH 9.8 (0.1 M CAPS buffer with 1 mM $MgCl_2$ and 0.5 M NaCl at pH 9.8) and 25 °C. VAP was allowed to react with ADP for 10 minutes

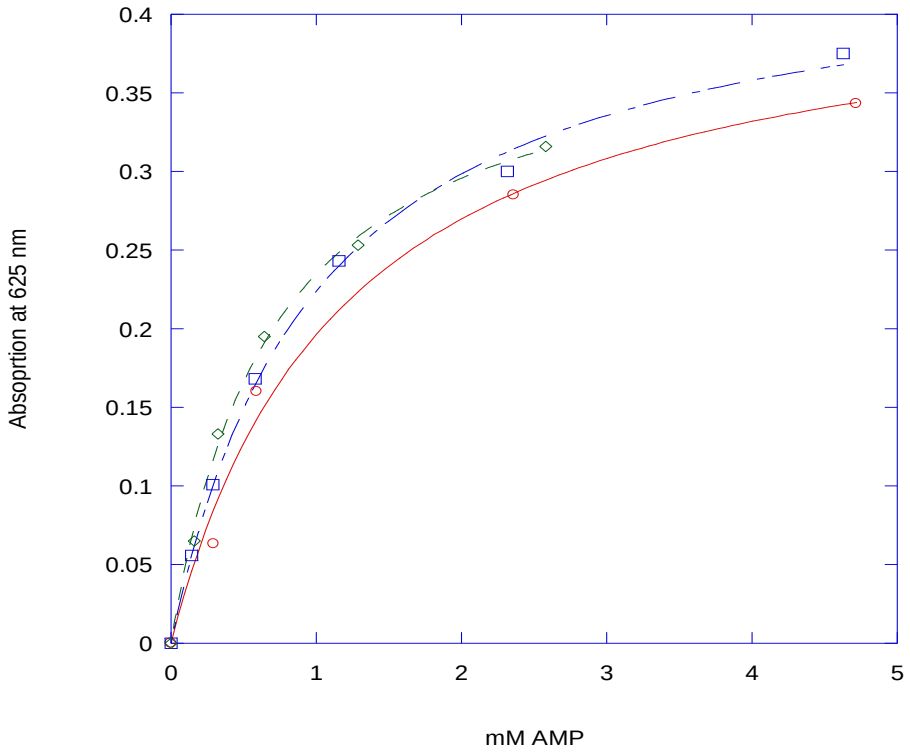

Figure 27: The Michaelis-Menten curve for ECAP when AMP was the substrate. The concentration of AMP was plotted against the absorbance at 625 nm (indicative of phosphate concentration). These curves from independent experiments were used to determine the turnover number and K_m value. The measurements were conducted at pH 9.8 (0.1 M CAPS buffer with 1 mM $MgCl_2$ and 0.5 M NaCl at pH 9.8) *and 25 °C. VAP was allowed to react with AMP for 20 minutes.*

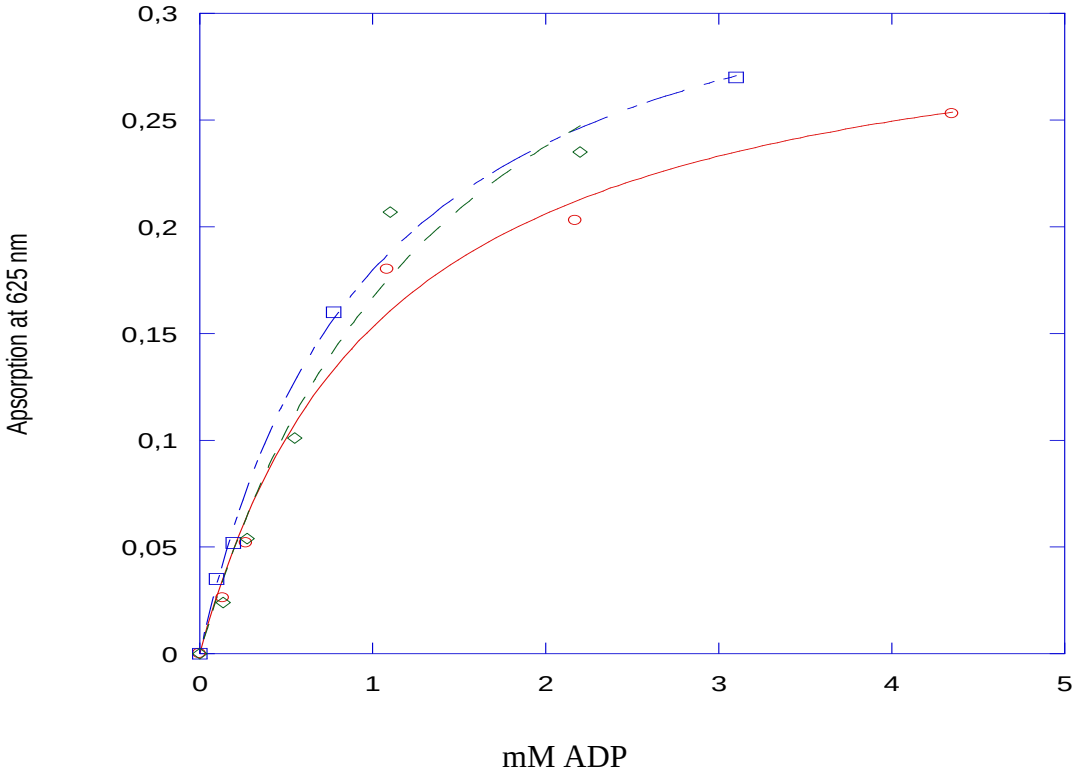

Figure 28: The Michaelis-Menten curve for ECAP when ADP was the substrate. The concentration of ADP is plotted against the absorbance at 625 nm (indicative of phosphate concentration). These curves from independent experiments where used to determine the turnover number and K_m value. The measurements were conducted at pH 9.8 (0.1 M CAPS buffer with 1 mM $MgCl_2$ and 0.5 M NaCl at pH 9.8) and 25 °C. VAP was allowed to react with ADP for 10 minutes

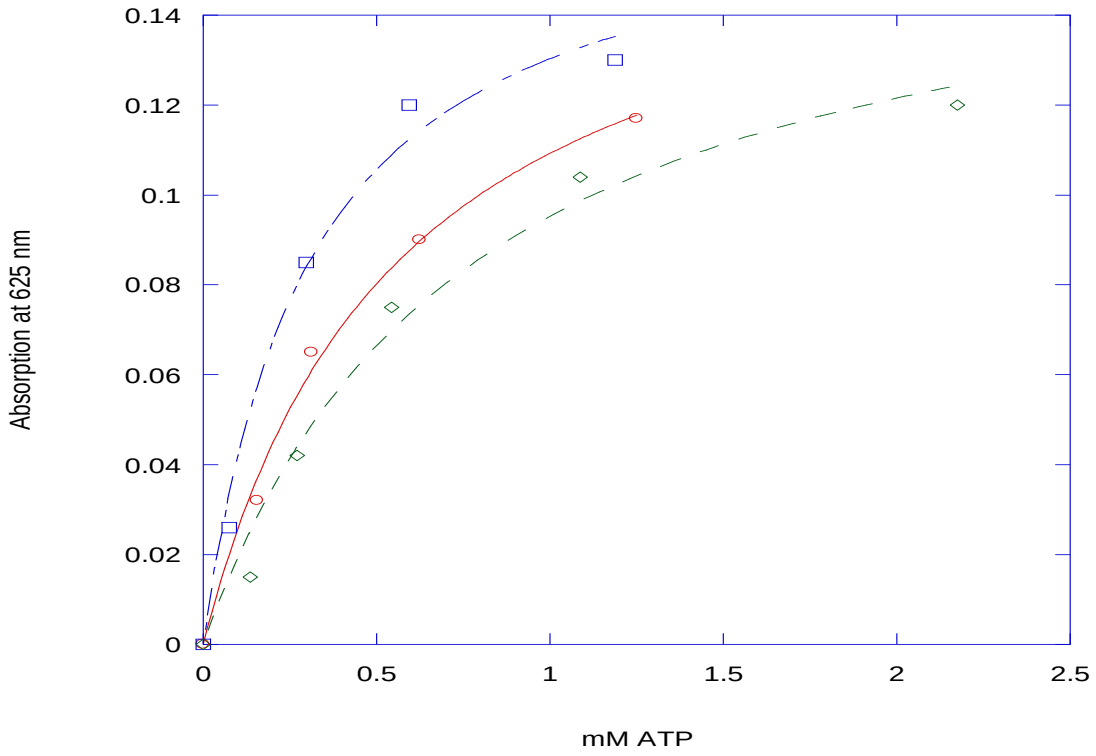

Figure 29: The Michaelis-Menten curve for ECAP when ATP was the substrate. The concentration of ATP is plotted against the absorbance at 625 nm (indicative of phosphate concentration). These curves from independent experiments where used to determine the turnover number and K_m value. The measurements were conducted at pH 9.8 (0.1 M CAPS buffer with 1 mM $MgCl_2$ and 0.5 M NaCl at pH 9.8) and 25 °C. VAP was allowed to react with ATP for 10 minutes

APPENDIX D

PyMol Commands.

http://www.pymolwiki.org/index.php/Selection_Algebra

Atom selection:

select bb, elem mg // selects magnesium atoms in the protein.

select resi, resi 1+2+3 // selects residues 1, 2 and 3

color red, resi 1 // color residue 1 red.

Hydrogen bonds:

h_addprot // add protons to structures

select don, (elem n, o and (neighbor hydro)) // creates selection don which includes nitrogen, //oxygen and neighboring hydrogens

select acc, (elem o or (elem n and not (neighbor hydro))) // creates selection don which //includes nitrogen, oxygen without neighboring hydrogens

dist HBA, (lig and acc),(prot and don), 3.2 // these commands show the hydrogen bonds //with minimally acceptable geometry. (Change 3.2 to 3.6) for ideal geometry

dist HBD, (lig and don),(prot and acc), 3.2

Electrostatic surface:

To prepare .dx file (needed to show the electrostatic surface of a protein in PyMol) visit http://nbcr-222.ucsd.edu/pdb2pqr_1.8/ and enter the pdb code and enter the desired pH value in the use PROPKA to assign protonation states at pH window.

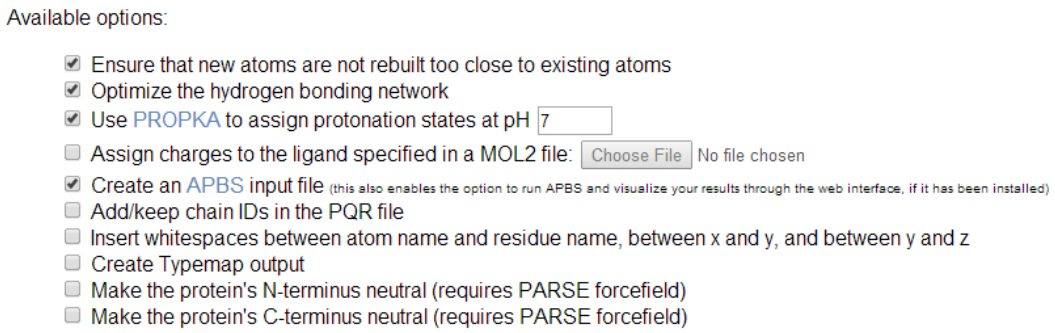

Figure 30. Available options found on http://nbcr-222.ucsd.edu/pdb2pqr_1.8/ *. To make .dx file select use Propka to assign protonated states and choose suitable pH value.*

The code for electrostatic surface is:

```
# load the molecules and maps
load firstmol.pdb  // load the .pdb file
loadfirstmap.dx // load the .dx file

# create the ramps and show the surfaces
ramp_new firstramp, firstmap, [-10,0,10]
setsurface_color, firstramp, 1ED9
show surface, 1ED9
```

Background setting:

bg_color white / / turns the background white

setray_opaque_background, off // transparent background.

APPENDIX E

Further results from AutoDockVina

When docking with Vina, the software returns a list of suitable conformations rather than only the one with the lowest binding free energy. This provides an opportunity for the researcher to compare multiple conformations in regard to number of hydrogen bonds and/ or other factors. In this project, I focused on the conformations with the lowest binding energy and they are the ones presented in this paper.

Table 11: The best modes of enzyme-ligand conformation as a result of docking VAP with ADP_ Model with AutoDockVina.

Mode	ΔG(kcal)/mol
1	-8.0
2	-8.0
3	-8.0
4	-7.8
5	-7.6
6	-7.6
7	-7.5
8	-7.2
9	-7.2

Table 12: The best modes of enzyme-ligand conformation as a result of docking VAP with AMP_ Ideal with AutoDock Vina.

Mode	ΔG(kcal)/mol
1	-7.8
2	-7.7
3	-7.6
4	-7.6
5	-7.6
6	-7.4
7	-7.4
8	-7.3
9	-7.2

Table 13: The best modes of enzyme-ligand conformation a result of docking VAP with ATP_ Model with AutoDock Vina.

Mode	ΔG(kcal)/mol
1	-8.1
2	-7.9
3	-7.9
4	-7.7
5	-7.6
6	-7.5
7	-7.3
8	-7.3
9	-7.3

Table 14: The results from enzyme-ligand conformation as a result of docking ECAP with AMP_ideal with AutoDock Vina.

Mode	ΔG(kcal)/mol
1	-4.9
2	-3.8
3	-3.4
4	-3.1
5	-2.8
6	-2.1
7	-2.1

Table 15: The results from enzyme-ligand conformation as a result of docking ECAP with ADP_model with AutoDock Vina.

Mode	ΔG(kcal)/mol
1	-5.7
2	-5.0

Table 16: The results from enzyme-ligand conformation as a result of docking ECAP with ATP_model with Atodock Vina.

Mode	ΔG(kcal)/mol
1	-1.8
2	-1.6